The Evolution of Protostars: Insights from Ten Years of Infrared Surveys with *Spitzer* and *Herschel*

Michael M. Dunham
Yale University; Harvard-Smithsonian Center for Astrophysics

Amelia M. Stutz
Max Planck Institute for Astronomy

Lori E. Allen
National Optical Astronomy Observatory

Neal J. Evans II
The University of Texas at Austin

William J. Fischer and S. Thomas Megeath
The University of Toledo

Philip C. Myers
Harvard-Smithsonian Center for Astrophysics

Stella S. R. Offner
Yale University

Charles A. Poteet
Rensselaer Polytechnic Institute

John J. Tobin
National Radio Astronomy Observatory

Eduard I. Vorobyov
University of Vienna; Southern Federal University

Stars form from the gravitational collapse of dense molecular cloud cores. In the protostellar phase, mass accretes from the core onto a protostar, likely through an accretion disk, and it is during this phase that the initial masses of stars and the initial conditions for planet formation are set. Over the past decade, new observational capabilities provided by the *Spitzer Space Telescope* and *Herschel Space Observatory* have enabled wide-field surveys of entire star-forming clouds with unprecedented sensitivity, resolution, and infrared wavelength coverage. We review resulting advances in the field, focusing both on the observations themselves and the constraints they place on theoretical models of star formation and protostellar evolution. We also emphasize open questions and outline new directions needed to further advance the field.

1. INTRODUCTION

The formation of stars occurs in dense cores of molecular clouds, where gravity finally overwhelms turbulence, magnetic fields, and thermal pressure. This review assesses the current understanding of the early stages of this process, focusing on the evolutionary progression from dense cores up to the stage of a star and disk without a surrounding envelope: the protostellar phase of evolution.

Because of the obscuration at short wavelengths by dust and the consequent re-emission at longer wavelengths, protostars are best studied at infrared and radio wavelengths, using both continuum emission from dust and spectral lines. At the time of the last Protostars and Planets conference,

only initial *Spitzer* results were reported and *Herschel* had not yet launched. For this review, we can incorporate much more complete *Spitzer* results and report on some initial *Herschel* results. We focus this review on the progress made with these facilities toward answering several key questions about protostellar evolution, as outlined below.

How do surveys find protostars and distinguish them from background galaxies, AGB stars, and more evolved star plus disk systems? What is the resulting census of protostars and young stars in nearby molecular clouds? Various identification methods have been employed and are compared in §2, leading to a much firmer census from relatively unbiased surveys of clouds in the Gould Belt and Orion.

How do we distinguish various stages in protostellar evolution? Theoretically, a collapsing core initially forms a first hydrostatic core, which quickly collapses again to form a true protostar, referred to as Stage 0. As material moves from the surrounding core to the disk and onto the star, the stellar mass eventually exceeds the core mass, and the system becomes a Stage I object. We discuss in §2 the observational correlatives to these Stages (called Classes) and the reliability of using observational signatures to distinguish between the Stages, while various candidates for the elusive first hydrostatic core are considered in §4.

How long do each of the observational Classes last? Ideally, we would ask this question about the Stages, but the issues addressed in §2 restrict current information about timescales to the Classes. With the large surveys now available and with careful removal of contaminants, we can now estimate durations of the observational Classes (§2,4).

What is the luminosity distribution of protostars (§2)? What histories of accretion are predicted by various theoretical and semi-empirical models, and how do these compare to the observations (§3)? Does accretion onto the star vary smoothly or is it more episodic? This question is addressed in significant detail in the accompanying chapter by *Audard et al*. Here we address it with respect to the luminosity distribution in §3, and other observational constraints are discussed in §5. While some results of monitoring are becoming available, most information on the protostellar accretion or luminosity variations comes from indirect proxies such as outflow patterns and chemical effects with timescales appropriate to reflect the luminosity evolution.

How does the disk form and evolve during the protostellar phase and how is this affected by the accretion history? This question is also addressed from a theoretical perspective in the accompanying chapter by *Li et al.*, so we focus in §6 on the observational evidence for and properties of disks in the protostellar phases.

What is the microscopic (chemical and mineralogical) evolution of the infalling material? Spectroscopy has provided information on the nature of the building blocks of comets and planetesimals as they fall toward the disk (§7).

What is the effect of the star forming environment? Protostars are found in a wide range of environments, ranging from isolated dense cores to low density clusters of cores in a clump, to densely clustered regions like Orion. These issues are addressed in §8.

The organization of this review chapter is motivated by first providing a very broad overview of the protostars that have been revealed by *Spitzer* and *Herschel* surveys (§2), followed by a general theoretical overview of the protostellar mass accretion process (§3). The rest of the review then focuses on specialized topics related to protostellar evolution, including the earliest stages of evolution (§4), the evidence for episodic mass accretion in the protostellar stage (§5), the formation and early evolution of protostellar disks (§6), the evolution of infalling material (§7), and the role of environment (§8).

2. PROTOSTARS REVEALED BY INFRARED SURVEYS

Within the nearest 500 pc, low-mass young stellar objects (YSOs) can be detected by modern instruments across most of the initial mass function over a wide range of wavelengths. Due to the emission from surrounding dust in envelopes and/or disks, YSOs are best identified at infrared wavelengths where all but the most embedded protostars are detectable (see §4). Older pre-main-sequence stars that have lost their circumstellar dust are not revealed in the infrared but can be identified in X-ray surveys (e.g., *Audard et al.*, 2007; *Winston et al.*, 2010; *Pillitteri et al.*, 2013).

Several large programs to detect and characterize YSOs have been carried out with the *Spitzer Space Telescope* (*Werner et al.*, 2004), which operated at 3–160 μm during its cryogenic mission. These include "From Molecular Cores to Planet-Forming Disks" (c2d; *Evans et al.*, 2003, 2009), which covered seven large, nearby molecular clouds and $\sim$100 isolated dense cores, the *Spitzer* Gould Belt Survey (*Dunham et al.*, 2013), which covered 11 additional nearby clouds, and *Spitzer* surveys of the Orion (*Megeath et al.*, 2012) and Taurus (*Rebull et al.*, 2010) molecular clouds. These same regions have recently been surveyed by a number of key programs with the far-infrared *Herschel Space Observatory* (*Pilbratt et al.*, 2010), which observed at 55–670 μm, including the *Herschel* Gould Belt Survey (*André et al.*, 2010) and HOPS, the *Herschel* Orion Protostar Survey (*Fischer et al.*, 2013; *Manoj et al.*, 2013; *Stutz et al.*, 2013). The wavelength coverage and resolution offered by *Herschel* allow a more precise determination of protostellar properties than ever before. Many smaller *Spitzer* and *Herschel* surveys have also been performed and their results will be referred to when relevant.

The results from these large surveys differ due to a combination of sample selection, methodology, sensitivity, resolution, and genuine differences in the star formation environments. While the last of these is of major scientific interest and is touched upon in §8, definitive evidence for differences in star formation caused by environmental factors awaits a rigorous combining of the samples and analysis with uniform techniques, which is beyond the scope of this review. Here we highlight the broad similarities and differences in the surveys.

2.1. Identification

YSOs are generally identified in the infrared by their red colors relative to foreground and background stars. Reliable identification is difficult since many other objects have similar colors, including star-forming galaxies, active galactic nuclei (AGN), background asymptotic giant branch (AGB) stars, and knots of shock-heated emission. Selection criteria based on position in various color-color and color-magnitude diagrams have been developed to separate YSOs from these contaminants and are described in detail by *Harvey et al.* (2007) for the c2d and Gould Belt surveys and by *Gutermuth et al.* (2009), *Megeath et al.* (2009, 2012), and *Kryukova et al.* (2012) for the Orion survey.

Once YSOs are identified, multiple methods are employed to pick out the subset that are protostars still embedded in and presumed to be accreting from surrounding envelopes. For the c2d and Gould Belt clouds, *Evans et al.* (2009) and *Dunham et al.* (2013) defined as protostars those objects with at least one detection at $\lambda \geq 350$ μm, with the rationale being that (sub)millimeter detections in typical surveys of star-forming regions trace surrounding dust envelopes but not disks due to the relatively low mass sensitivities of these surveys (see *Dunham et al.*, 2013). On the other hand, *Kryukova et al.* (2012) identified protostars in the c2d, Taurus, and Orion clouds using a set of color and magnitude criteria designed to pick out objects with the expected red colors of protostars, but they did not require (sub)millimeter detections. A comparison of the two samples shows general agreement except for a large excess of faint protostars in the *Kryukova et al.* (2012) sample.

This discrepancy in the number of faint protostars may be due to incompleteness in the *Dunham et al.* (2013) sample, whose requirement of a (sub)millimeter detection may have introduced a bias against the lowest-mass cores and thus the lowest-mass (and luminosity) protostars. It may also be due to unreliability of some detections by *Kryukova et al.* (2012), whose corrections for contamination from galaxies, edge-on disks, and highly extinguished Class II YSOs is somewhat uncertain, especially at the lowest luminosities where contamination steeply rises. Both effects likely contribute. Resolution of this discrepancy should be possible in the near future once complete results from the *Herschel* and James Clerk Maxwell Telescope SCUBA-2 Legacy Gould Belt surveys are available, since together they will fully characterize the population of dense cores in all of the Gould Belt clouds with sensitivities below 0.1 $M_\odot$. This general trade-off of completeness versus reliability remains the subject of ongoing study, with *Hsieh and Lai* (2013) recently presenting a new method of identifying YSOs in *Spitzer* data that may increase the number of YSOs by $\sim$30% without sacrificing reliability. We anticipate continued developments in the coming years.

2.2. Classification

The modern picture of low-mass star formation resulted from the merger of an empirical classification scheme with theoretical work on the collapse of dense, rotating cores (e.g., *Shu et al.*, 1987; *Adams et al.*, 1987; *Wilking et al.*, 1987; *Kenyon et al.*, 1993), and was reviewed by *White et al.* (2007) and *Allen et al.* (2007) at the last Protostars and Planets conference. In this picture there are three stages of evolution after the initial starless core. In the first, the protostellar stage, an infalling envelope feeds an accreting circumstellar disk. In the second, the envelope has dissipated, leaving a protoplanetary disk that continues to accrete onto the star. In the third, the star has little or no circumstellar material, but it has not yet reached the main sequence. Defining S_λ as the flux density at wavelength λ, *Lada* (1987) used the infrared spectral index,

$$\alpha = \frac{d\log(\lambda S_\lambda)}{d\log\lambda} \quad , \tag{1}$$

to divide objects into three groups – Class I, II, and III – meant to correspond to these three stages. *Greene et al.* (1994) added a fourth class, the "Flat-SED" sources (see §2.4), leading to the following classification system:

- Class I: $\alpha \geq 0.3$
- Flat-SED: $-0.3 \leq \alpha < 0.3$
- Class II: $-1.6 \leq \alpha < -0.3$
- Class III: $\alpha < -1.6$

Class 0 objects were later added as a fifth class for protostars too deeply embedded to detect in the near-infrared but inferred through other means (i.e., outflow presence; *Andre et al.*, 1993). They were defined observationally as sources with a ratio of submillimeter to bolometric luminosity ($L_{\rm smm}/L_{\rm bol}$) greater than 0.5%, where $L_{\rm smm}$ is calculated for $\lambda \geq 350$ μm. Fig. 1 shows example SEDs for a starless core and for Class 0, Class I, and Flat-SED sources as well as several other types of objects that will be discussed in subsequent sections. For the first time, *Spitzer* and *Herschel* surveys of star-forming regions have provided truly complete spectral coverage for most protostars.

Due to the effects of inclination, aspherical geometry, and foreground reddening, there is not a one-to-one correspondence between observational Class and physical Stage (e.g., *Whitney et al.*, 2003a,b; *Robitaille et al.*, 2006; *Crapsi et al.*, 2008). To avoid confusion, *Robitaille et al.* (2006) proposed the use of Stages 0, I, II, and III when referring to the physical or evolutionary status of an object and the use of "Class" only when referring to observations. We follow this recommendation throughout this review.

While the original discriminant between Class 0 and I protostars is $L_{\rm smm}/L_{\rm bol}$, this quantity has historically been difficult to calculate because it requires accurate submillimeter photometry. Another quantity often used in its place is the bolometric temperature ($T_{\rm bol}$): the effective temperature of a blackbody with the same flux-weighted mean frequency as the observed SED (*Myers and Ladd*, 1993). $T_{\rm bol}$ begins near 20 K for deeply embedded protostars (*Launhardt et al.*, 2013) and eventually increases to the effective temperature of a low-mass star once all of the surrounding

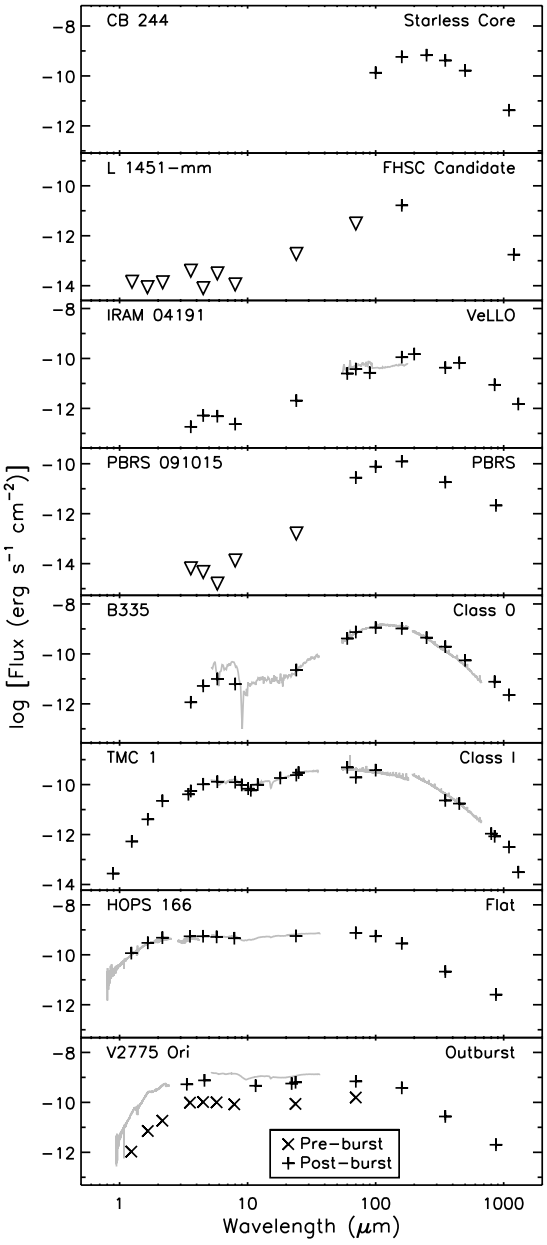

Fig. 1.— SEDs for a starless core (*Stutz et al.*, 2010; *Launhardt et al.*, 2013), a candidate first hydrostatic core (*Pineda et al.*, 2011), a very low-luminosity object (*Dunham et al.*, 2008; *Green et al.*, 2013b), a PACS bright red source (*Stutz et al.*, 2013), a Class 0 protostar (*Stutz et al.*, 2008; *Launhardt et al.*, 2013; *Green et al.*, 2013b), a Class I protostar (*Green et al.*, 2013b), a Flat-SED source (*Fischer et al.*, 2010), and an outbursting Class I protostar (*Fischer et al.*, 2012). The + and × symbols indicate photometry, triangles denote upper limits, and gray lines show spectra.

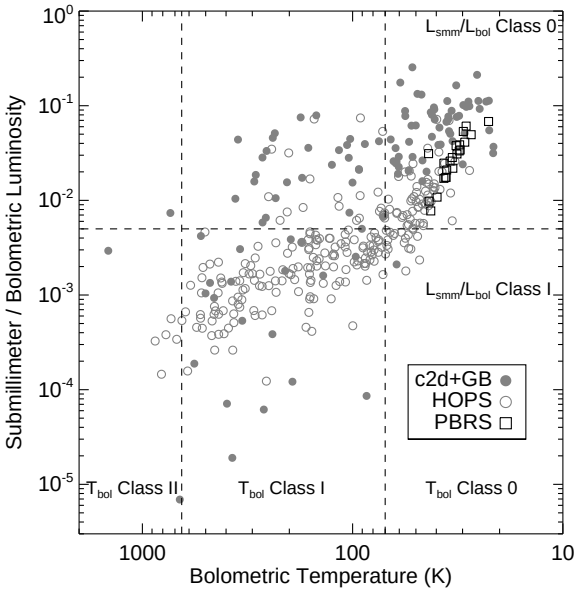

Fig. 2.— Comparison of $L_{\rm smm}/L_{\rm bol}$ and $T_{\rm bol}$ for the protostars in the c2d, GB, and HOPS surveys. The PBRS (§4.2.3) are the 18 Orion protostars that have the reddest 70 to 24 μm colors, 11 of which were discovered with *Herschel*. The dashed lines show the Class boundaries in $T_{\rm bol}$ from *Chen et al.* (1995) and in $L_{\rm smm}/L_{\rm bol}$ from *Andre et al.* (1993). Protostars generally evolve from the upper right to the lower left, although the evolution may not be monotonic if accretion is episodic.

core and disk material has dissipated. *Chen et al.* (1995) proposed the following Class boundaries in $T_{\rm bol}$: 70 K (Class 0/I), 650 K (Class I/II), and 2800 K (Class II/III).

With the sensitivity of *Spitzer*, Class 0 protostars are routinely detected in the infrared, and Class I sources by α are both Class 0 and I sources by $T_{\rm bol}$ (*Enoch et al.*, 2009). Additionally, sources with flat α have $T_{\rm bol}$ consistent with Class I or Class II, extending roughly from 350 to 950 K, and sources with Class II and III α have $T_{\rm bol}$ consistent with Class II, implying that $T_{\rm bol}$ is a poor discriminator between α-based Classes II and III (*Evans et al.*, 2009).

$T_{\rm bol}$ may increase by hundreds of K, crossing at least one Class boundary, as the inclination ranges from edge-on to pole-on (*Jorgensen et al.*, 2009; *Launhardt et al.*, 2013; *Fischer et al.*, 2013). Thus, many Class 0 sources by $T_{\rm bol}$ may in fact be Stage I sources, and vice versa. Far-infrared and submillimeter diagnostics have a superior ability to reduce the influence of foreground reddening and inclination on the inferred protostellar properties. At such wavelengths foreground extinction is sharply reduced and observations probe the colder, outer parts of the envelope that are less optically thick and thus where geometry is less important. Flux ratios at $\lambda \geq 70$ μm respond primarily to envelope density, pointing to a means of disentangling these effects and developing more robust estimates of evolutionary stage (*Ali et al.*, 2010; *Stutz et al.*, 2013). Along these lines, several authors have recently argued that $L_{\rm smm}/L_{\rm bol}$ is a better tracer of underlying physical Stage than $T_{\rm bol}$ (*Young and Evans*, 2005; *Dunham et al.*, 2010a; *Launhardt et al.*, 2013).

Recent efforts have vastly expanded the available 350 μm data for protostars via, e.g., the *Herschel* Gould Belt survey (see accompanying chapter by *André et al.*), several *Herschel* key programs (e.g., *Launhardt et al.*, 2013; *Green et al.*, 2013b), and ground-based observations (e.g.,

Wu et al., 2007). These efforts have enabled accurate calculation of $L_{\rm smm}/L_{\rm bol}$ for large samples. Fig. 2 compares classification via $L_{\rm smm}/L_{\rm bol}$ and $T_{\rm bol}$ for the c2d, GB, and HOPS protostars. While there are methodology differences in the details of how $L_{\rm smm}$ is calculated for the c2d+GB (*Dunham et al.*, 2013) and HOPS (*Stutz et al.*, 2013) protostars that must be resolved in future studies, the two classification methods agree 81% of the time (counting $T_{\rm bol}$ Class II and $L_{\rm smm}/L_{\rm bol}$ Class I as agreement). In a similar analysis of nine isolated globules, *Launhardt et al.* (2013) did not find such a clear agreement between $T_{\rm bol}$ and $L_{\rm smm}/L_{\rm bol}$ classification, although methodology and possibly environmental differences are substantial (*Launhardt et al.*, 2013). Between the increased availability of submillimeter data and the evidence that $L_{\rm smm}/L_{\rm bol}$ is a better tracer of underlying physical Stage, we suggest using $L_{\rm smm}/L_{\rm bol}$ rather than $T_{\rm bol}$ as the primary tracer of the evolutionary status of protostars. However, the concept of monotonic evolution through the observational Classes breaks down if accretion is episodic (see §3, 5). Instead, protostars will move back and forth across class boundaries as their accretion rates and luminosities change (*Dunham et al.*, 2010a).

Table 1 lists the numbers of YSOs classified via α for the c2d+GB, Orion, and Taurus surveys. Since portions of Orion suffer from incompleteness, we present data for subregions where the counts are most complete (L1630 and L1641). Additionally, due to the high extinction toward Orion, we present for this region both the total number of Flat-SED sources as well as the number that are likely reddened Stage II objects based on analysis of longer-wavelength data. Not included are new protostars in Orion discovered by *Herschel* (see §4.2.3); including these increases the total number by only 5%–8%, emphasizing that *Spitzer* surveys missed relatively few protostars.

Table 1 also gives lifetimes for the protostellar (Class 0+I) and Flat-SED objects. These are calculated under the following set of assumptions: (1) time is the only variable, (2) star formation is continuous over at least the assumed Class II lifetime, and (3) the Class II lifetime is 2 Myr (see the accompanying chapter by *Soderblom et al.*). This lifetime is best thought of as a "half-life" rather than an absolute lifetime. Averaged over all surveys, we derive a protostellar lifetime of ∼0.5 Myr. While the flat-SED lifetime by this analysis is ∼0.4 Myr, this class may be an inhomogeneous collection of objects that are not all YSOs at the end of envelope infall (§2.4). In all cases these are lifetimes of *observed classes* rather than *physical stages*, since the latter are not easily observable quantities. Indeed, some recent theoretical studies suggest the true lifetime of the protostellar stage may be shorter than the lifetime for the Class 0+I protostars derived here (*Offner and McKee*, 2011; *Dunham and Vorobyov*, 2012).

Table 1: YSO Numbers and Lifetimes

	c2d+GB	L1630[a]	L1641[b]	Taurus
Numbers				
Class 0+I[c]	384	51	125	26
Flat	259	48	131	22
Flat[d]	···	30	74	···
Class II	1413	243	559	125
Lifetimes[e]				
Class 0+I (Myr)	0.54	0.42	0.45	0.42
Flat (Myr)	0.37	0.40	0.47	0.35
Class 0+I (Myr)[f]	···	0.37	0.39	···
Flat (Myr)[f]	···	0.13	0.18	···

[a] Omitting regions of high nebulosity
[b] Omitting the Orion Nebula region
[c] Not including new Herschel sources
[d] Number of previous row that are likely reddened Class II
[e] Assuming a Class II lifetime of 2 Myr (see text)
[f] Counting sources in row marked *d* as Class II

2.3. Protostellar Luminosities

Fig. 3 plots $L_{\rm bol}$ vs. $T_{\rm bol}$ (a "BLT" diagram; *Myers and Ladd*, 1993) for the protostars in the c2d+GB and Orion surveys, along with the separate $L_{\rm bol}$ and $T_{\rm bol}$ distributions. The 220 c2d+GB protostars are the YSOs in those surveys with submillimeter detections. The 332 Orion protostars are the 317 identified by *Megeath et al.* (2012) that were detected in HOPS 70 μm observations, plus an additional 15 that were newly discovered by HOPS (§4.2.3; *Stutz et al.*, 2013). Bolometric properties were calculated by trapezoidal integration under the available SEDs with no extrapolation to shorter or longer wavelengths and no corrections for foreground extinction. As found in previous work (*Kenyon et al.*, 1990), the luminosity distribution extends over several orders of magnitude, but this is now the case for hundreds of sources, and the distributions extend to even lower luminosities. Explanations for these broad distributions will be evaluated in §3.

Statistics for the $L_{\rm bol}$ distributions appear in Table 2. Since the flux completeness limits of the c2d, GB, and HOPS surveys can be a function of position in regions with diffuse emission, and the relationship between source fluxes and $L_{\rm bol}$ depends on distance, source evolutionary status, local strength of the external radiation field, and total core mass available to be heated externally, it is difficult to derive an exact completeness limit in $L_{\rm bol}$. *Dunham et al.* (2013) derive an approximate completeness limit of 0.05 $L_\odot$ for all but the most distant cloud in the c2d and GB surveys (IC5146), which increases to 0.2 $L_\odot$ when IC5146 is included. A full analysis of the HOPS completeness limit is still under investigation (*Stutz et al.*, in preparation).

The c2d+GB distribution extends over three orders of magnitude. Except for a statistically significant excess of low luminosity Class I sources, the distributions are generally similar for Classes 0 and I. Looking at the same clouds, *Kryukova et al.* (2012) find a distribution shifted to lower luminosities, with a mean (median) of 0.66 (0.63) $L_\odot$. The discrepancy between these two studies is partially resolved by updating the empirical relationship adopted by *Kryukova*

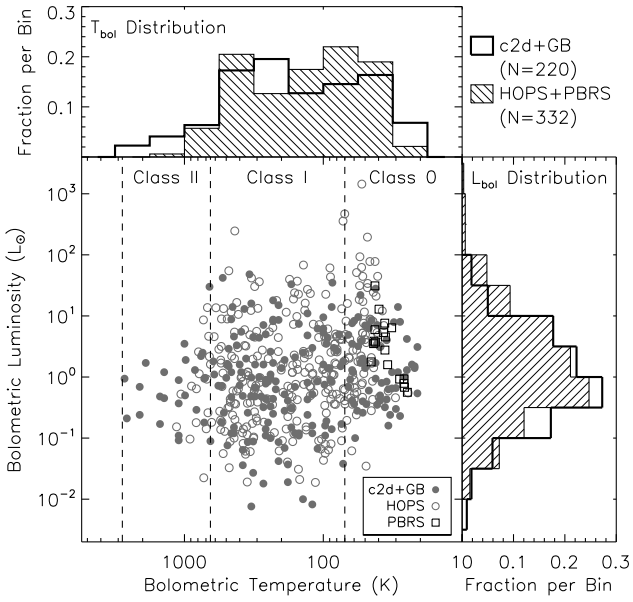

Fig. 3.— The combined bolometric luminosity vs. temperature (BLT) diagram for the 552 protostars identified in the c2d, Gould Belt, and Spitzer Orion / HOPS surveys. BLT properties are measured by integrating under the observed SEDs. Marginal distributions of $T_{\rm bol}$ and $L_{\rm bol}$ are shown as histograms. The full population of protostars spans more than four orders of magnitude in luminosity.

Table 2: Protostellar $L_{\rm bol}$ Statistics ($L_\odot$)

	c2d+GB	HOPS
Range	0.01–69	0.02–1440
Mean (Median)	4.3 (1.3)	14 (1.2)
Class 0 Mean (Median)	4.5 (1.4)	27 (3.5)
Class I Mean (Median)	3.8 (1.0)	9.3 (1.0)

NOTE: Classes are by $T_{\rm bol}$. See text for details on which sources are counted as protostars and included here.

et al. (2012) to calculate $L_{\rm bol}$, but some discrepancy remains (*Dunham et al.*, 2013). As discussed above, there are concerns with both the completeness of *Dunham et al.* (2013) and the reliability of *Kryukova et al.* (2012).

Including new *Herschel* sources, the HOPS distribution extends over four orders of magnitude, with thirteen protostars that are more luminous than the most luminous c2d+GB source. These sources increase the mean values of the HOPS luminosty distribution for both the Class 0 and I subsamples by factors of 6 and 2.4, respectively, and also increase the median Class 0 luminosity by a factor of 2.5 compared to the c2d+GB value. The degree to which these changes can be attributed to environmental differences as opposed to incompleteness effects in the various samples is currently under investigation (*Stutz et al., in preparation*).

2.4. Refining the Timeline of Protostellar Evolution

Determining when (and how quickly) envelopes dissipate is a major constraint for theories of how mass accretes

Table 3: Protostellar Numbers by $T_{\rm bol}$

	c2d+GB	HOPS
Class 0	63	93
Class I	132	222
Fraction of Class 0[a]	0.32	0.30
Lifetime of Class 0 (Myr)[b]	0.16	0.15

[a] Ratio of Class 0 to Class 0+I

[b] Ratio multiplied by the 0.5 Myr Class 0+I lifetime

onto protostars (see §3). One key metric is the relative numbers (and thus implied durations) of Class 0 and I protostars, which should be sensitive to the accretion history. We list the numbers of each in Table 3, using $T_{\rm bol}$ for classification since not all of the c2d and GB protostars have sufficient data for reliable $L_{\rm smm}/L_{\rm bol}$ calculations. We find that 30% of protostars are in Class 0 based on $T_{\rm bol}$ (*Enoch et al.*, 2009; *Dunham et al.*, 2013; *Fischer et al.*, 2013), implying a Class 0 lifetime of 0.15 Myr, but interpreting these results is complicated by the lack of a one-to-one correspondence between Class and Stage. The combination of ubiquitous high-sensitivity far-infrared and submillimeter observations and improved modeling possible in the *Herschel* and ALMA eras will lead to a better understanding of the relative durations of these Stages.

In this review we have quoted a derived protostellar duration of ∼0.5 Myr. However, the true duration remains uncertain. On one hand, some recent observations suggest that up to 50% of Class I YSOs may be highly reddened Stage II objects (*van Kempen et al.*, 2009; *Heiderman et al.*, 2010), a possibility also discussed by *White et al.* (2007). However, the exact fraction is uncertain and may have been overestimated by these studies. On the other hand, the nature of the Flat-SED sources is unclear and has not yet been well-determined in the literature. Some of them may represent objects in transition between Stages I and II (e.g., *Calvet et al.*, 1994), but determining their exact nature is critical for determining the duration of the protostellar stage. Future work on this front is clearly needed. Finally, all the timescales discussed in this chapter scale directly with the timescale for the Class II phase, which we have assumed to be 2 Myr (see the accompanying chapters on the ages of young stars by *Soderblom et al.* and on transitional disks by *Espaillat et al.* for further discussion of this timescale).

3. PROTOSTELLAR ACCRETION

The fundamental problem of star formation is how stars accrete their mass. In this section we give a general theoretical overview of how stars gain their masses and discuss the challenges of modeling protostellar luminosities. Understanding protostellar properties and evolution depends upon both the macrophysics of the core environment and the microphysics that drives gas behavior close to the protostar. After discussing protostellar luminosities (§3.1), we describe three categories of models: those that depend on

core properties (§3.2), those that are based on the core environment and feedback (§3.3), and those focused on accretion disk evolution (§3.4). This separation is mainly for clarity since actual protostellar accretion is determined by a variety of nonlinear and interconnected physical processes that span many orders of magnitude in density and scale.

3.1. The Protostellar Luminosity Problem

The luminosity of a protostar provides an indirect measure of two quantities: the instantaneous accretion rate and the protostellar structure. Unfortunately, the luminosity contributions of each are difficult to disentangle. Over the past two decades various theories have attempted and failed to explain observed protostellar luminosites, which are found to be generally ∼10 times less luminous than expected (*Kenyon et al.*, 1990; *Kenyon and Hartmann*, 1995; *Young and Evans*, 2005; *Evans et al.*, 2009). This discrepancy became known as the "protostellar luminosity problem" and can be stated as follows. The total protostellar luminosity is given by:

$$L_p = L_{\rm phot} + f_{\rm acc}\frac{Gm\dot{m}}{r}, \qquad (2)$$

where $L_{\rm phot}$ is the photospheric luminosity generated by deuterium burning and Kelvin-Helmholtz contraction, m is the protostellar mass, $\dot{m}$ is the instantaneous accretion rate, r is the protostellar radius, and $f_{\rm acc}$ is the fraction of energy radiated away in the accretion shock. For accretion due to gravitational collapse (e.g., *Stahler et al.* 1980), $\dot{m} \sim (c_s^2 + v_A^2 + v_t^2)^{3/2}/G \simeq 10^{-5}\,{\rm M}_\odot\ {\rm yr}^{-1}$, where c_s, v_A, and v_t are the sound, Alfvén, and turbulent speeds, respectively. Given a typical protostellar radius $r = 3.0\ {\rm R}_\odot$ (*Stahler*, 1988; *Palla and Stahler*, 1992), the accretion luminosity of a 0.25 $\rm M_\odot$ protostar is $\sim 25\ {\rm L}_\odot$. This is many times the observed median value and is only a lower limit to the true problem since it neglects the contributions from $L_{\rm phot}$ and from external heating by the interstellar radiation field.

However, Eq. 2 contains several poorly constrained quantities. The accretion rate onto a protostar is due to a combination of infalling material driven by gravitational collapse on large scales and the transport of material through an accretion disk on small scales. The disk properties are set by the core properties and the rate of infall (e.g., *Vorobyov*, 2009a; *Kratter et al.*, 2010a, see also the accompanying chapter by *Li et al.*), and significant theoretical debate continues on the relationship between infall through the core and accretion onto the protostar, both instantaneously and averaged over time. Although it is difficult to directly measure $\dot{m}$, estimates for T Tauri stars based on infrared emission lines suggest $\dot{m} \lesssim 10^{-7}\ {\rm M}_\odot\ {\rm yr}^{-1}$ (e.g., *Muzerolle et al.*, 1998). Based on observational estimates for the embedded lifetime (see §2), it is not possible for protostars to reach typical stellar masses without significantly higher average accretion during the embedded phase. While similar measurements of infrared emission lines in the protostellar phase are especially difficult, some observations suggest similarly low rates for Class I objects (e.g., *Muzerolle et al.*, 1998; *White et al.*, 2007). Presently it is unclear if such observations are representative of all protostars or instead biased toward those objects already near the end of the protostellar stage and thus detectable in the near-infrared. A higher accretion rate is inferred in at least one protostar from its current accretion luminosity and mass derived from the Keplerian velocity profile of its disk (*Tobin et al.*, 2012). Mass infall rates derived from millimeter molecular line observations are also typically higher (e.g., *Brinch et al.*, 2009; *Mottram et al.*, 2013), although such rates are only available for some sources and are highly model-dependent.

The intrinsic stellar parameters are also poorly constrained. While main-sequence stellar evolution is relatively well understood, pre-main sequence evolution, especially during the first few Myr, is much less well-constrained. Consequently, both $L_{\rm phot}$ and r are uncertain and depend on the properties of the first core, past accretion history, accretion shock physics, and the physics of stellar interiors (*Baraffe et al.*, 2009; *Hosokawa et al.*, 2011; *Baraffe et al.*, 2012).

The luminosity problem was first identified by *Kenyon et al.* (1990), who also proposed several possible solutions, including slow and episodic accretion. In the slow accretion scenario, the main protostellar accretion phase lasts longer than a freefall time, which was then typically assumed to be ∼0.1 Myr. Current observations suggest a protostellar duration of ~ 0.5 Myr (§2), which helps to alleviate the problem. In the episodic accretion scenario, accretion is highly variable and much of the mass may be accreted in statistically rare bursts of high accretion, observational evidence for which is discussed in §5 and in the accompanying chapter by *Audard et al.* One additional solution concerns the radiative efficiency of the accretion shock. If some of the shock kinetic energy is absorbed by the star or harnessed to drive outflows such that $f_{\rm acc} < 1$ (e.g., *Ostriker and Shu* 1995), the radiated energy would be reduced. Recent models applying combinations of these solutions have made significant progress towards reconciling theory and observation, as discussed in the remainder of this Section.

3.2. Core-Regulated Accretion

A variety of theoretical models have been proposed for the gravitational collapse of dense cores. These models predict quantities such as the core density profile, gas velocities and, most crucially, the rate of mass infall to the core center. If the accretion rate of a forming protostar is identical to the gas infall rate, as expected in models where disks either efficiently transfer mass onto the protostar or do not form at all, then these models also predict protostellar accretion rates. Numerical simulations of forming clusters suggest that accretion rates predicted by theoretical models are on average comparable to the stellar accretion rate (e.g., *Krumholz et al.*, 2012). In this section and in §3.3 we discuss models that assume that the accreting gas is efficiently channeled from 0.1 pc to 0.1 AU scales, equivalent to fo-

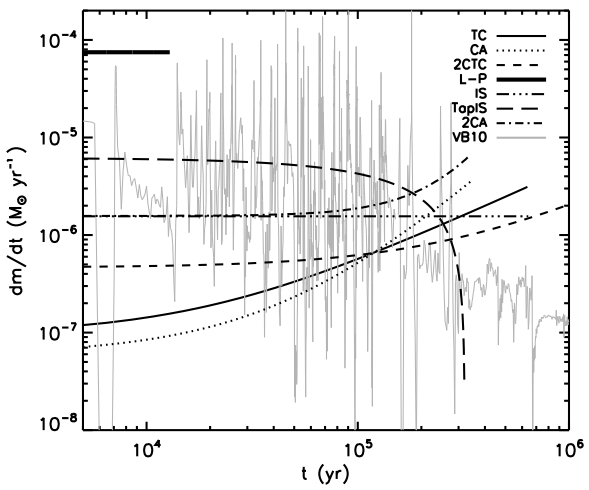

Fig. 4.— Various model accretion rates as a function of time for a star of final mass 1 $M_\odot$. The models are the turbulent core (TC), competitive accretion (CA), two-component turbulent core (2CTC), Larson-Penston (L-P), isothermal sphere (IS), tapered isothermal sphere (TapIS), two-component accretion (2CA), and a simulated accretion history from *Vorobyov and Basu* (2010a). The TC, CA and 2CTC are computed assuming a mean formation time of $\langle t_f \rangle = 0.44$ Myr.

cusing on the time-averaged accretion rate. Models where the instantaneous and time-averaged accretion rates may diverge significantly are discussed in §3.4.

Fig. 4 illustrates the accretion rate versus time for a 1 $M_\odot$ star for a variety of theoretical models. Most core-regulated accretion models are based on the assumption that gas collapses from a local dense reservoir of order ∼0.1 pc, i.e., a "core". The collapse of an isothermal, constant density sphere including thermal pressure is the simplest model with a self-similar solution. *Larson* (1969) and *Penston* (1969) separately calculated the resulting accretion rate to be $\dot{m} = 46.9 c_s^3/G = 7.4 \times 10^{-5} (T/10\mathrm{K})^{3/2} \mathrm{M}_\odot$ yr^{-1}, where c_s and T are the thermal sound speed and temperature, respectively. The self-similar solution for the collapse of a centrally condensed, isothermal sphere was computed by *Shu* (1977), who found $\dot{m} = 0.975 c_s^3/G$, a factor of ∼50 less than the Larson-Penston solution. In both cases, accretion does not depend on the initial mass, which leads to the prediction that accretion rate is independent of the instantaneous protostellar and final stellar mass and implies that the only environmental variable that affects accretion is the local gas temperature.

The above models consider only thermal pressure and gravity. However, cores are observed to be both magnetized and somewhat turbulent. The most massive clumps (e.g., *Barnes et al.* 2011), which are possible progenitors of massive protostars, have turbulent linewidths several times the thermal linewidth. *McKee and Tan* (2003) proposed a "turbulent core" model to account for the higher column densities and turbulent linewidths of high-mass cores. In this model, $\dot{m} \propto m^{1/2} {m_f}^{3/4}$, where m and m_f are the instantaneous and final protostellar masses, respectively.

Significant numerical work has been devoted to modeling the formation of star clusters (see the accompanying chapter by *Offner et al*). Many of these simulations present a very dynamical picture in which protostellar accretion rates vary as a function of location within the global gravitational potential and protostars "compete" with one another for gas (*Bonnell et al.*, 2001). The most massive stars form in the center of the gravitational potential where they can accrete at high rates. Protostars accrete until the gas is either completely accreted or dispersed, leading to a constant accretion time for all stars that is proportional to the global freefall time. Analytically, this suggests $\dot{m} \propto m^{2/3} m_f$ (*Bonnell et al.*, 2001; *McKee and Offner*, 2010).

All core-regulated accretion models then fall somewhere between the limits of constant accretion rate and constant star formation time. *McKee and Offner* (2010) propose hybrid models that include both a turbulent and a thermal component ("two-component turbulent core") or a competitive and a thermal component ("two-component competitive accretion"). Additional models have sought to analytically include rotation (*Terebey et al.*, 1984), nonzero initial velocities (*Fatuzzo et al.*, 2004), and magnetic fields (*Adams and Shu*, 2007). For example, *Adams and Shu* (2007) modify the isothermal sphere collapse problem to consider ambipolar diffusion. They derive accretion rates that are enhanced by a factor of 2-3 relative to the non-magnetized case.

Declining accretion rates that fall by an order of magnitude or more from their peak are produced in some numerical simulations (*Vorobyov and Basu*, 2008; *Offner et al.*, 2009). *McKee and Offner* (2010) model this decline by imposing a "tapering" factor, $(1 - t/t_f)$, such that accretion declines and terminates at some specified formation time, t_f. Infall could also be variable due to turbulence or magnetic effects (e.g., *Tassis and Mouschovias*, 2005), but such scenarios have not been well studied theoretically and are observationally difficult to constrain.

3.3. Feedback-Regulated Accretion

Most stars are born in cores in extended molecular clouds that are surrounded by lower-density filamentary gas and other recently formed protostars (e.g., *Bergin and Tafalla*, 2007; *Evans et al.*, 2009). These core environments provide mass for accretion from beyond the core, and "stellar feedback" in the form of ionizing radiation, winds and outflows may also disperse star-forming gas. In this case the core environment is important, and the initial core mass is not sufficient to predict the final protostar mass. Instead the protostar mass depends on its accretion history and the competition between infall and dispersal.

Early models of such feedback-regulated accretion concentrated on the competition between accretion and outflows (*Norman and Silk*, 1980). *Basu and Jones* (2004) proposed a lognormal distribution of initial core masses, whose accretion rates are proportional to their mass, and accretion

durations follow a waiting-time distribution. For this distribution, the probability density that accretion endures for t and then stops between t and $t + dt$ is $(1/\tau)e^{-t/\tau}$, where τ is the mean accretion duration. A similar distribution of accretion durations was proposed to describe ejections by small multiple systems (*Bate and Bonnell*, 2005).

Recently, *Myers* (2010) proposed a feedback-regulated model that accounts for protostellar masses that follow the IMF. The basic ideas of the model are (1) protostars accrete from core-clump condensations, (2) the duration of accretion is the most important factor in setting the final mass of a protostar, and (3) accretion durations vary due to a combination of ejections, dispersal by stellar feedback, accretion competition, and exhaustion of initial gas. The waiting-time distribution describes this combination.

In dense clusters, a promising direction for protostar mass models is to treat the mass accretion rate as a function of mass or time, rather than as due to the collapse of a particular initial configuration. This approach allows discrimination between various IMF-forming accretion models (see also §3.2). *Myers* (2009b, 2010) formulate a two-component accretion rate denoted "2CA" having a constant, thermal component and a mass-dependent component (see Fig. 4). The 2CA accretion rate is similar to that of the two-component turbulent core model. *Myers* (2010) combined this 2CA model with an explicit distribution of accretion durations to derive the protostellar mass distribution and showed that it closely resembles the stellar IMF.

3.4. Disk-Regulated Accretion

Since most core mass likely accretes through a disk (§6), it is important to determine how this mass is redistributed within the disk and transported onto the star. Two main processes of mass and angular momentum transport in disks have been proposed: viscous torques due to turbulence triggered by the magneto-rotational instability (MRI) (*Balbus and Hawley*, 1991) and gravitational torques induced by gravitational instability (GI) (*Lin and Pringle*, 1987; *Laughlin and Bodenheimer*, 1994). Which of these mechanisms dominates and the efficiency with which the disk transports mass onto the protostar (and thus the degree to which the instantaneous infall and accretion rates are coupled) are currently debated and may depend on the details of local physical conditions, including the core properties and the infall rate. Numerical models that circumvent the complicated physics of the MRI and GI and treat both as a local viscous transport mechanism have been developed based on the *Shakura and Sunyaev* (1973) α-parameterization. These α-disk models have been successful in describing many aspects of disk physics and accretion (e.g., *Kratter et al.*, 2008; *Zhu et al.*, 2009), though their applicability may be limited for fairly massive disks (*Vorobyov*, 2010).

The MRI is known to operate only if the ionization fraction is sufficiently high to couple the magnetic field with the gas (*Blaes and Balbus*, 1994). Protostellar disks are sufficiently cold and dense that known ionization sources (thermal, X-rays, cosmic rays) may fail to provide the ionization needed to sustain the MRI, particularly in the disk mid-plane. If this is the case, *Gammie* (1996) proposed that the MRI may be active only in a layer near the surface, an idea known as "layered accretion". Various disk models suggest that the so-called dead zone, wherein the MRI is largely suppressed, may occupy a significant fraction of the disk volume at AU scales (see review by *Armitage*, 2011).

On the other hand, analytic models and numerical hydrodynamics simulations indicate that the physical conditions in protostellar disks may be favorable for the development of GI (*Toomre*, 1964; *Lin and Pringle*, 1987; *Laughlin and Bodenheimer*, 1994). Whenever the destabilizing effect of self-gravity becomes comparable to the stabilizing effects of pressure and shear, spiral density waves develop. If heating due to GI is balanced by disk cooling, the disk settles into a quasi-steady state in which GI transports angular momentum outwards allowing mass to accrete onto the central star (*Lodato and Rice*, 2004). In this picture, gravitational torques alone are sufficient to drive accretion rates consistent with observations of intermediate- and upper-mass T Tauri stars (*Vorobyov and Basu*, 2007, 2008). However, for the very low-mass disks around low-mass stars and brown dwarfs, GI is likely to be suppressed and, consequently, viscous mass transport due to MRI alone may explain the accretion rates of these objects (*Vorobyov and Basu*, 2009).

The degree of GI depends on a number of factors including the angular momentum of the parent core, infall rate, disk mass, and amount of radiative heating from the central protostar (*Kratter et al.*, 2010a; *Offner et al.*, 2010; *Vorobyov and Basu*, 2010a; *Stamatellos et al.*, 2011). If the disk is relatively massive and the local disk cooling time is faster than the dynamical time, sections of spiral arms can collapse into bound fragments and lead to a qualitatively different mode of disk evolution. In this mode, disk accretion is an intrinsically variable process due to disk fragmentation, nonaxisymmetric structure, and gravitational torques (*Vorobyov*, 2009b). Fragments that form in the disk outer regions are quickly driven inwards due to the loss of angular momentum via gravitational interaction with the spiral arms (*Vorobyov and Basu*, 2005, 2006; *Baruteau et al.*, 2011; *Cha and Nayakshin*, 2011). As they accrete onto the protostar, clumps trigger luminosity bursts similar in magnitude to FU-Orionis-type or EX-Lupi-type events (*Vorobyov and Basu*, 2005, 2006, 2010a; *Machida et al.*, 2011a).

This burst mode of accretion mostly operates in the embedded phase of protostellar evolution when the continuing infall of gas from the parent core triggers repetitive episodes of disk fragmentation. The mass accretion onto the burgeoning protostar is characterized by short ($\lesssim 100-200$ yr) bursts with accretion rate $\dot{m} \gtrsim$ a few $\times\, 10^{-5} M_\odot$ yr^{-1} alternated with longer ($10^3 - 10^4$ yr) quiescent periods with $\dot{m} \lesssim 10^{-6} M_\odot$ yr^{-1} (*Vorobyov and Basu*, 2010a). After the parent core is accreted or dispersed, any remaining fragments may trigger final accretion bursts or survive to form wide-separation planets or brown dwarfs (*Vorobyov and Basu*, 2010b; *Kratter et al.*, 2010b; *Vorobyov*, 2013).

Gravitational fragmentation is one of many possible mechanisms that can generate accretion and luminosity bursts (see accompanying chapter by *Audard et al.*). Among the other mechanisms, a combination of MRI and GI has been most well-studied (*Zhu et al.*, 2009, 2010; *Martin et al.*, 2012). In this scenario, GI in the outer disk transfers gas to the inner sub-AU region where it accumulates until the gas density and temperature reach values sufficient for thermal ionization to activate the MRI. The subsequent enhanced angular momentum transport triggers a burst of accretion. The GI+MRI burst mechanism may act in disks that are not sufficiently massive to trigger disk fragmentation, but the details of the MRI are still poorly understood. Independent of their physical origin, luminosity bursts have important implications for disk fragmentation, accretion, and theoretical models of star formation.

3.5. Comparison between Models and Observations

Here, we consider direct comparisons between observations and several theoretical models.

3.5.1. Protostellar Luminosities

In order to consider the luminosity problem, *McKee and Offner* (2010) developed an analytic formalism for the present-day protostellar mass function (PMF). The PMF depends on the instantaneous protostellar mass, final mass, accretion rate, and average protostellar lifetime. Given some model for protostellar luminosity as a function of protostellar properties, *Offner and McKee* (2011) then derived the present-day protostellar luminosity function (PLF). Since the PLF depends only on observable quantities such as the protostellar lifetime and on a given theoretical model for accretion, the PLF can be used to directly compare star formation theories with observations.

Offner and McKee (2011) computed the predicted PLFs for a variety of models and parameters, including the isothermal sphere, turbulent core, competitive accretion, and two-component turbulent core models. Fig. 5 compares the observed protostellar luminosity distribution with some of these predicted PLFs where the accretion rate is allowed to taper off as the protostar approaches its final mass. Models in which the accretion rate depends on the final mass (such as the turbulent core or competitive accretion models) naturally produce a broad distribution of luminosities. *Offner and McKee* (2011) also found that the theoretical models actually produce luminosities that are *too dim* compared to observations, given an average formation time of $\langle t_f \rangle \sim 0.5$ Myr and allowing for episodic accretion. They concluded that a star formation time of $\langle t_f \rangle \simeq 0.3$ Myr provides a better match to the mean and median observed luminosities.

On the other hand, given that numerical simulations of disk evolution indicate that protostellar accretion may be an intrinsically variable process, the wide spread in the observed protostellar luminosity distribution may result from large-scale variations in the protostellar accretion rate (*Dunham et al.*, 2010a). This idea was further developed by *Dunham and Vorobyov* (2012), who used numerical hydrodynamics simulations of collapsing cores coupled with radiative transfer calculations to compare the model and observed properties of young embedded sources in the c2d clouds. They showed that gravitationally unstable disks with accretion rates that both decline with time and feature short-term variability and episodic bursts can reproduce the full spread of observations, including very low luminosity objects. As shown in Fig. 5, accretion variability induced by GI and disk fragmentation can thus provide a reasonable match to the observed protostellar luminosity distribution and resolve the long-standing luminosity problem.

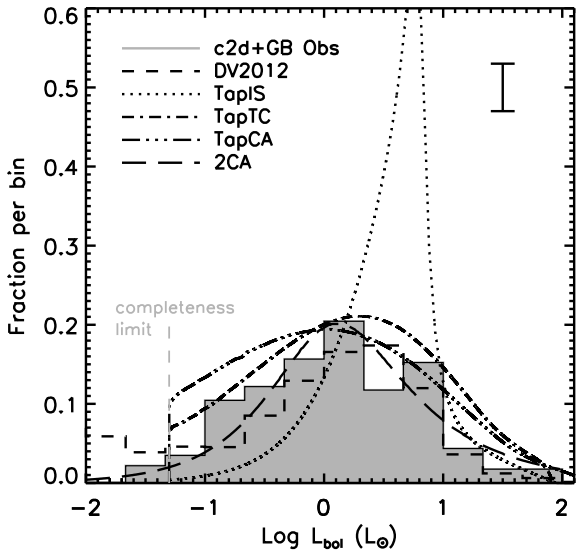

Fig. 5.— Distribution of extinction-corrected protostellar luminosities from the c2d+GB surveys (shaded), predicted from disk simulations (dash, *Dunham and Vorobyov*, 2012), tapered Isothermal Sphere (dots), tapered Turbulent Core (dot-dash), tapered Competitive Accretion (dot-dot-dash, *Offner and McKee*, 2011), and two-component accretion (long dash, *Myers*, 2012). The tapered models adopt a completeness limit of 0.05 $L_\odot$. Typical observational uncertainties are shown in the upper right.

Finally, the distribution of protostellar masses can be obtained for the case of feedback-regulated accretion by combining the two-component accretion (2CA) model with an explicit distribution of accretion times. *Myers* (2011, 2012) used the corresponding distribution of masses and accretion rates to compute the predicted PLF and found that it is in reasonable agreement with the observed protostellar luminosity distribution in nearby clouds.

3.5.2. Ages of Young Clusters

Models which specify accretion durations can also be tested against age estimates of young clusters. Such models can predict as a function of time the number of cluster members which are protostars, since they are still accreting, and the number which are pre-main sequence stars (PMS),

since they have stopped accreting. Application of the 2CA model to embedded cluster members identified as protostars or PMS indicate typical cluster ages of 1-3 Myr, in good agreement with estimates from optical and infrared spectroscopy and pre-main sequence evolutionary tracks. This method can be used to date obscured young subclusters that are inaccessible to optical spectroscopy (*Myers*, 2012).

3.5.3. Future Work

The models described above provide tangible, diverse resolutions to the luminosity problem, including mass-dependent and highly-variable accretion histories. Future observational work should concentrate on constraining the magnitude and timescales of protostellar variability to assess its effects on protostellar luminosities and, ultimately, its importance in the mass accretion process. On the theoretical front, high resolution global-disk simulations, which include protostellar heating, magnetization, and ionization are needed to improve our understanding of disk-regulated accretion variability. Improved theoretical understanding of outflow launching and evolution is needed to interpret observed outflow variability and how it correlates with accretion. Additional synthetic observations of models that take into account the complex, asymmetric morphologies of accreting protostars and the effects of external heating are required to properly compare to observed luminosities. Finally, dust evolution and chemical reaction networks determine the distribution of species, which is the lens through which we perceive all observational results. Many theoretical studies gloss over or adopt simplistic chemical assumptions, which undermines direct comparison between theory and observation.

4. THE EARLIEST OBSERVABLE STAGES OF PROTOSTELLAR EVOLUTION

The identification of young stars in the very earliest stages of formation is motivated by the goals of studying the initial conditions of the dense gas associated with star formation before modification by feedback and of determining the properties of cores when collapse begins. The earliest theoretically predicted phases are the first hydrostatic core and Stage 0 protostars. Observational classes of young objects include Class 0 sources, very low luminosity objects (VeLLOs; §4.2.1), candidate first hydrostatic cores (FHSC; §4.2.2), and PACS bright red sources (PBRS; §4.2.3). The challenge is to unambiguously tie observations to theory, a process complicated by optical depth effects, geometric (inclination) degeneracies, and intrinsically faint and/or very red observed SEDs. We begin with a theoretical overview of the earliest stages of evolution and then follow with observational anchors provided by *Spitzer*, *Herschel*, and other facilities.

4.1. Theoretical framework

Once a dense molecular cloud core begins to collapse, the earliest object that forms is the first hydrostatic core (first core, FHSC). First predicted by *Larson* (1969), the FHSC exists between the starless and protostellar stages of star formation and has not yet been unambiguously identified by observations. The FHSC forms once the central density increases to the point where the inner region becomes opaque to radiation ($\rho_c \gtrsim 10^{-13}$ g cm^{-3}; *Larson*, 1969), rendering the collapse adiabatic rather than isothermal. This object continues to accrete from the surrounding core and both its mass and central temperature increase with time. Once the temperature reaches $\sim$ 2000 K, the gravitational energy liberated by accreting material dissociates H_2, preventing the temperature from continuing to rise to sufficiently balance gravity. At this point the second collapse is initiated, leading to the formation of the second hydrostatic core, more commonly referred to as the protostar.

Table 4: Predicted properties of FHSCs

Property	Range	References
Maximum Mass [$M_\odot$]	$0.04 - 0.05$	1, 2, 3, 4
	$0.01 - 0.1^a$	5, 6
Lifetime [kyr]	$0.5 - 50$	1, 3, 4, 6, 7
Internal Luminosity [$L_\odot$]	$10^{-4} - 10^{-1}$	2, 3
Radius [AU]	~ 5	2
	$\gtrsim 10 - 20^a$	5, 6

[a] With the effects of rotation included.

References: (1) *Boss and Yorke* (1995); (2) *Masunaga et al.* (1998); (3) *Omukai* (2007); (4) *Tomida et al.* (2010); (5) *Saigo and Tomisaka* (2006); (6) *Saigo et al.* (2008); (7) *Commerçon et al.* (2012a)

The current range in predicted FHSC properties are summarized in Table 4. The significant variation in predicted properties is largely driven by different prescriptions and assumptions about magnetic fields (e.g., *Commerçon et al.*, 2012a), rotation (e.g., *Saigo and Tomisaka*, 2006; *Saigo et al.*, 2008), and accretion rates. Rotation may produce a flattened, disk–like morphology for the entire FHSC (*Saigo and Tomisaka*, 2006; *Saigo et al.*, 2008), implying that disks may actually form before protostars with masses larger than the protostars themselves (*Bate*, 2011; *Machida and Matsumoto*, 2011).

Studies of FHSC SEDs have shown that the emitted radiation is completely reprocessed by the surrounding envelope, with SEDs characterized by emission from $10 - 30$ K dust and no observable emission below $\sim 20 - 50$ μm (*Boss and Yorke*, 1995; *Masunaga et al.*, 1998; *Omukai*, 2007; *Saigo and Tomisaka*, 2011). Emission profiles in various molecular species and simulated ALMA continuum images (*Saigo and Tomisaka*, 2011; *Tomisaka and Tomida*, 2011; *Commerçon et al.*, 2012b; *Aikawa et al.*, 2012) demonstrate the critical value of additional observational constraints beyond continuum SEDS. *Machida et al.* (2008) showed that first cores drive slow (~ 5 km s^{-1}) outflows with wide opening–angles while *Price et al.* (2012) showed that, under certain assumptions, first core outflows may show strong collimation. Future theoretical attention is

needed. Indeed, despite the dire observational need, no clear and unambiguous predictions for how a first core can be differentiated from a very young protostar have yet been presented.

4.2. Observations

Here we outline recent observational developments in the identification of the youngest sources, focusing on discoveries of three classes of observationally defined objects mentioned above: Very low luminosity objects (VeLLOs), candidate FHSCs, and PACS bright red sources (PBRS).

4.2.1. ***Very Low Luminosity Objects (VeLLOs)***

Prior to the launch of *Spitzer*, dense cores were identified as protostellar or starless based on the presence or absence of an associated *IRAS* detection. Beginning with *Young et al.* (2004), *Spitzer* c2d observations revealed a number of faint protostars in cores originally classified as starless. This led to the definition of a new class of objects called very low luminosity objects (VeLLOs): protostars embedded in dense cores with internal luminosities $L_{\rm int} \leq 0.1$ L$_\odot$ (*di Francesco et al.*, 2007), where $L_{\rm int}$ excludes the luminosity arising from external heating by the interstellar radiation field. A total of 15 VeLLOs have been identified in the c2d regions (*Dunham et al.*, 2008), with six the subject of detailed observational and modeling studies (*Young et al.*, 2004; *Dunham et al.*, 2006; *Bourke et al.*, 2006; *Lee et al.*, 2009b; *Dunham et al.*, 2010b; *Kauffmann et al.*, 2011).

The above studies have postulated three explanations for VeLLOs, whose very low luminosities require very low protostellar masses and/or accretion rates: (1) Extremely young protostars with very little mass yet accreted, (2) Older protostars observed in quiescent periods of a cycle of episodic accretion, and (3) Proto-brown dwarfs. The properties of the host cores and outflows driven by VeLLOs vary greatly from source to source, suggesting that VeLLOs (which are defined observationally) do not correspond to a single evolutionary stage and are instead a heterogeneous mixture of all three possibilities listed above. While the relatively strong mid-infrared detections guarantee that none are first hydrostatic cores, at least some VeLLOs are consistent with being extremely young Class 0 protostars just beyond the end of the first core stage (see §4.2.2).

4.2.2. ***Candidate First Hydrostatic Cores***

Nine other objects embedded within cores originally classified as starless have been detected and identified as candidate first cores. These objects have been revealed through faint mid–infrared detections of compact sources below the sensitivities of the large *Spitzer* surveys (*Belloche et al.*, 2006; *Enoch et al.*, 2010), (sub)millimeter detections of molecular outflows driven by "starless" cores (*Chen et al.*, 2010; *Pineda et al.*, 2011; *Schnee et al.*, 2012; *Chen et al.*, 2012; *Murillo and Lai*, 2013), and far–infrared detections indicating the presence of warm dust heated by an internal source (*Pezzuto et al.*, 2012). However, we caution that even the very existence of some of these objects remains under debate (e.g., *Schmalzl et al.* 2013, in prep.).

Two significant questions have emerged: 1) Are any candidates true first cores? 2) How many "starless" cores are truly starless? The answer to the first question is not yet known; none clearly stand out as the best candidate(s) for a bona–fide FHSC, with arguments for and against each. Nonetheless, it is extremely unlikely that all are FHSC. Six of the nine candidate FHSCs are located in the Perseus molecular cloud. *Enoch et al.* (2009) identified 66 protostars in Perseus. Assuming that the duration of the protostellar stage is $\sim$0.5 Myr (§2) and a first core lifetime of $0.5 - 50$ kyr, as quoted above, we expect that there should be between 0.07 – 7 first cores in Perseus. Thus, unless the very longest lifetime estimates are correct, at least some (and possibly all) are very young second cores (protostars). Such objects would also be consistent with the definition of a VeLLO, emphasizing that these classes of objects are defined observationally and are not necessarily mutually exclusive in terms of evolutionary stage.

The number of "starless" cores that are truly starless is found by combining results for VeLLOs and candidate first cores. Combined, *Dunham et al.* (2008) and *Schnee et al.* (2012) find that approximately 18% – 38% of cores classified as starless prior to the launch of *Spitzer* in 2003 in fact harbor low–luminosity sources, although the exact statistics are still quite uncertain.

4.2.3. ***PACS Bright Red Sources (PBRS)***

Using HOPS *Herschel* 70 μm imaging, *Stutz et al.* (2013) searched for new protostars in Orion that were too faint at $\lambda \leq 24$ μm to be identified by *Spitzer*. They found 11 new objects with 70 μm and 160 μm emission that were either faint ($m(24) > 7$ mag) or undetected at $\lambda \leq 24$ μm. In addition, they found seven previously *Spitzer* identified protostars with equally red colors ($\log \lambda F_\lambda(70)/\lambda F_\lambda(24) > 1.65$). These 18 PBRS are the reddest known protostars in Orion A and Orion B. Fig. 6 shows five representative PBRS.

Although the emission at $\lambda \leq 24$ μm is faint for all PBRS, some are detected at 3.6–8.0 μm with *Spitzer*. These detections may be due to scattered light and shocked gas in outflow cavities, indicating the presence of outflows. A total of eight PBRS are undetected by *Spitzer* at 24 μm, leading to a lower limit for their $\lambda F_\lambda(70)/\lambda F_\lambda(24)$ color. At $\lambda \geq 70$ μm all PBRS have SEDs that are well characterized by modified black–bodies (see Fig. 1 for a representative PBRS SED). The mean 70 μm flux of the PBRS is similar to that of the rest of the HOPS sample of protostars, with a comparable but somewhat smaller spread in values.

The overall fraction of PBRS to protostars in Orion is $\sim$5%. Assuming PBRS represent a distinct phase in protostellar evolution (see further discussion of this assumption in §4.3), and further assuming a constant star formation rate and a protostellar duration of $\sim$0.5 Myr (§2), the implied duration of the PBRS phase is $\sim$25 kyr, averaging over

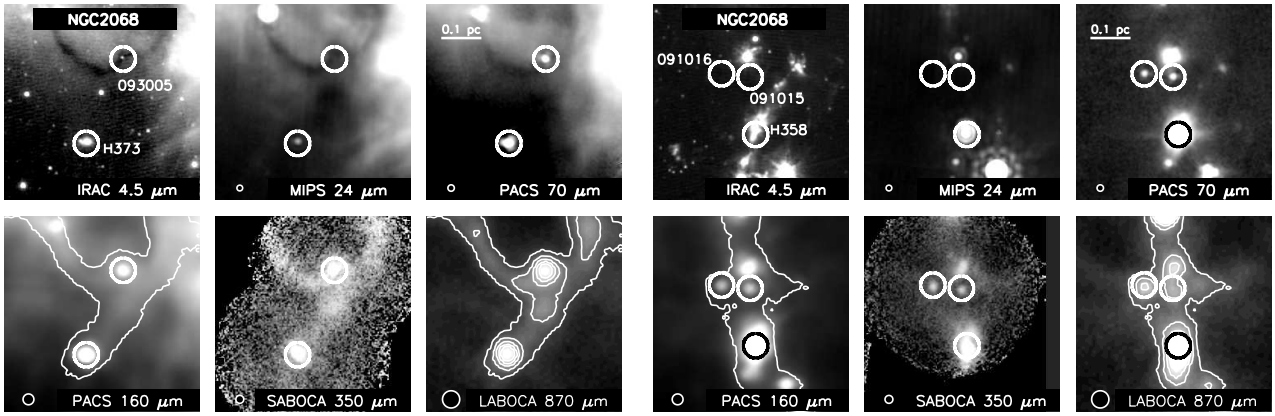

Fig. 6.— $4' \times 4'$ images of 5 PBRS at the indicated wavelengths. *Left:* PBRS 093005 and H373. Source 093005 is the reddest PBRS and therefore the reddest embedded object known in Orion, and lies at the intersection of three filaments seen in both absorption (8, 24, and 70 μm) and in emission (350 and 870 μm). *Right:* PBRS 091015, 019016, and H358. Figure adapted from *Stutz et al.* (2013).

all Orion regions. However, the spatial distribution of the PBRS displays a striking non–uniformity compared to the distribution of normal HOPS protostars: only 1% of the protostars in Orion A are PBRS, compared to ∼17% in Orion B. Whether this large variation in the spatial distribution indicates a recent burst of star formation or environmental differences remains to be determined.

Basic parameters of interest include $L_{\rm bol}$, $T_{\rm bol}$, and $L_{\rm smm}/L_{\rm bol}$, as well as modified black–body fits to the long–wavelength SEDs. The PBRS $L_{\rm bol}$ and $T_{\rm bol}$ distributions are shown in Fig. 3; $L_{\rm bol}$ spans a typical range compared to other protostars but $T_{\rm bol}$ is restricted to very low values ($T_{\rm bol} \leq 44$ K). Similarly, $L_{\rm smm}/L_{\rm bol}$ values for PBRS occupy the extreme high end of the distribution for all protostars in Orion (*Stutz et al.*, 2013, see Fig. 2). Modified black–body fits to the thermal portions of their SEDS yield PBRS envelope mass estimates in the range of ~ 0.2 — 1.0 M$_\odot$. Radiative transfer models confirm that the 70 μm detections are inconsistent with externally heated starless cores and instead require the presence of compact internal objects. While the overall fraction of PBRS relative to protostars in Orion is small (∼5%, see above), they are significant for their high envelope densities. Indeed, the PBRS have $70/24$ colors consistent with very high envelope densities, near the expected Class 0/I division or higher. The above evidence points toward extreme youth, making PBRS one of the few observational constraints we have on the earliest phases of protostellar evolution, all at a common distance with a striking spatial distribution within Orion.

4.3. Synthesis of Observations

With the discoveries of VeLLOs, candidate FHSC, and PBRS, these large *Spitzer* and *Herschel* surveys of star-forming regions have expanded protostellar populations to objects that are both less luminous and more deeply embedded than previously known. These three object types are defined observationally, often based on serendipitous discoveries, and are not necessarily mutually exclusive in terms of the physical stages of their constituents. All are likely heterogeneous samples encompassing true first cores and protostars of varying degrees of youth. Indeed, some of the lowest luminosity PBRS may in fact be first cores, and others with low luminosities are consistent with the definition of VeLLOs. Furthermore, at least some, and possibly all, of the objects identified as candidate first cores may not be true first cores but instead young protostars that have already evolved beyond the end of the first core stage. Such objects would be consistent with the definition of VeLLOs since they all have low luminosities, and some may be detected as PBRS once *Herschel* observations of the Gould Belt clouds are published. Integrating these objects into the broader picture of protostellar evolution is of great importance and remains a subject of on-going study. Further progress in characterizing the evolutionary status of these objects and using them as probes of the earliest stages of star formation depend on specific theoretical predictions for distinguishing between first cores and very young protostars followed by observations that test such predictions.

5. PROTOSTELLAR ACCRETION BURSTS AND VARIABILITY

There is a growing body of evidence that the protostellar accretion process is variable and punctuated by short bursts of very rapid accretion (the "episodic accretion" paradigm). Indeed, optical variability was one of the original, defining characteristics of a young stellar object (*Joy*, 1945; *Herbig*, 1952). We provide here a summary of the observational evidence for episodic mass accretion in the protostellar stage.

5.1. Variability, Bursts, and Flares in Protostars

There are two general classes of outbursting young stars known, FU Orionis type objects (FUors) and EX Lupi type

objects (EXors), which differ in their outburst amplitudes and timescales (see accompanying chapter by *Audard et al*). As an example of an outbursting source, Fig. 1 shows pre- and post-outburst SEDs of V2775 Ori, an outbursting protostar in the HOPS survey area (*Fischer et al.*, 2012). Based on the current number of known outbursting young stars, and assuming that all protostars undergo repeated bursts, *Offner and McKee* (2011) estimate that approximately 25% of the total mass accreted during the protostellar stage does so during such bursts. Some of the outbursting young stars detected to date are clearly still in the protostellar stage of evolution (e.g., *Fischer et al.*, 2012; *Green et al.*, 2013a, also see the accompanying chapter by *Audard et al.*), but whether or not all protostars undergo large-amplitude accretion bursts remains an open question.

Infrared monitoring campaigns offer the best hope for answering this question (e.g., *Johnstone et al.*, 2013), although we emphasize that not all detected variability is due to accretion changes; detailed modeling is necessary to fully constrain the variability mechanisms (e.g., *Flaherty et al.*, 2012, 2013). *Carpenter et al.* (2001) and *Carpenter et al.* (2002) studied the near-infrared variability of objects in the Orion A and Chamaeleon I molecular clouds and identified numerous variable stars in each. *Morales-Calderón et al.* (2011) presented preliminary results from YSOVAR, a *Spitzer* warm mission program to monitor young clusters in the mid-infrared, in which they identified over 100 variable protostars. Once published, the final results of the program should provide robust statistics on protostellar variability (*Morales-Calderón et al.*, 2011, *Rebull et al.*, 2013, in prep.). *Wolk et al.* (2013) found a variability fraction of 84% among YSOs in Cygnus OB7 with two-year near-infrared monitoring. *Megeath et al.* (2012) found that 50% of the YSOs in L1641 in Orion exhibited mid-infrared variability, with a higher fraction among the protostars alone compared to all YSOs, in multi-epoch *Spitzer* data spanning $\sim$ 6 months. *Billot et al.* (2012) presented *Herschel* far-infrared monitoring of 17 protostars in Orion and found that 8 (40%) show $>$10% variability on timescales from 10 – 50 days, which they attributed to accretion variability. Finally, *Findeisen et al.* (2013) report results from the Palomar Transient Factory optical monitoring of the North American and Pelican Nebulae. By monitoring at optical wavelengths they are very incomplete to the protostars in these regions, but all three of the protostars they detect show variability.

Another approach is to compare observations from different telescopes, which provides longer time baselines but introduces uncertainties from differing bandpasses and instrument resolutions. Three such studies have recently been published, although none had sufficient statistics to restrict their analysis to only protostars. *Kóspál et al.* (2012) compared *ISO* and *Spitzer* spectra for 51 young stars and found that 79% show variability of at least 0.1 magnitudes, and 43% show variability of at least 0.3 magnitudes, with all of the variability existing on timescales of about a year or shorter. *Scholz* (2012) compared 2MASS and UKIDDS near-infrared photometry with a time baseline of 8 years for 600 young stars and found that 50% show $>2\sigma$ variability and 3% show $>$0.5 magnitude variability, with the largest amplitudes seen in the youngest star-forming regions. Based on their statistics they derived an interval of at least 2000 – 2500 years between successive bursts. *Scholz et al.* (2013) compared *Spitzer* and *WISE* photometry with 5 year time baselines for 4000 young stars and identified 1 – 4 strong burst candidates with $>$1 magnitude increases between the two epochs. Based on these statistics they calculated a typical interval of 10,000 years between bursts.

At present, neither direct monitoring campaigns nor comparison of data from different telecopes at different epochs offer definitive statistics on protostellar variability or the role variability plays in shaping the protostellar luminosity distribution. However, they do demonstrate that variability is common among all YSOs, and protostars in particular, and they do offer some of the first statistical constraints on variability and burst statistics. We anticipate continued progress in this field in the coming years.

5.2. Accretion Variability Traced by Outflows

Molecular outflows are driven by accretion onto protostars and are ubiquitous in the star formation process (see accompanying chapter by *Frank et al.*). Any variability in the underlying accretion process should directly correlate with variability in the ejection process. Indeed, many outflows show clumpy structure that can be interpreted as arising from separate ejection events. Although such clumpy structures can also arise from the interaction between outflowing gas and a turbulent medium even in cases where the underlying ejection process is smooth (*Offner et al.*, 2011), many outflows with such structure also display kinematic evidence of variability. In particular, outflow clumps in molecular CO gas, which are often spatially coincident with near-infrared H_2 emission knots, are found at higher velocities than the rest of the outflowing gas, and within these clumps the velocities follow Hubble laws (increasing velocity with increasing distance from the protostar). This creates distinct structures in position-velocity diagrams called "Hubble wedges" by *Arce and Goodman* (2001), which are consistent with theoretical expectations for prompt entrainment of molecular gas by an episodic jet (e.g., *Arce and Goodman*, 2001, and references therein). One of the most recent examples of this phenomenon is presented by *Arce et al.* (2013) for the HH46/47 outflow using ALMA data and is shown in Fig. 7. The timescales of the episodicity inferred from the clump spacings and velocities range from less than 100 years to greater than 1000 years (e.g., *Bachiller et al.*, 1991; *Lee et al.*, 2009a; *Arce et al.*, 2013).

Additional evidence for accretion variability comes from the integrated properties of molecular outflows. In a few cases, low luminosity protostars drive strong outflows implying higher *time-averaged* accretion rates traced by the integrated outflows than the *current* rates traced by the protostellar luminosities (*Dunham et al.*, 2006, 2010b; *Lee*

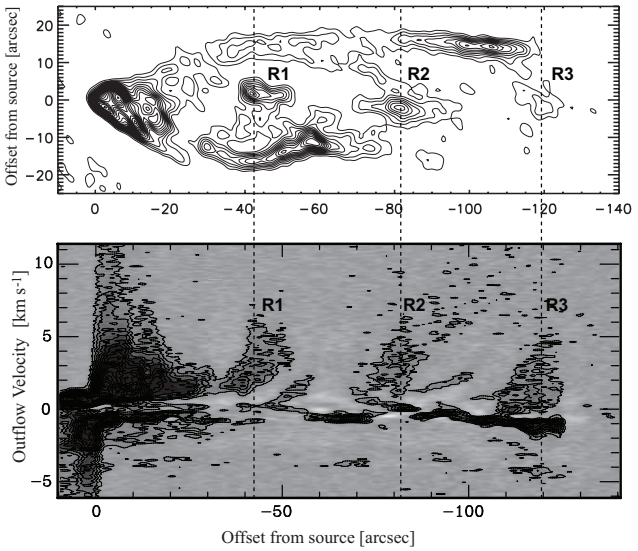

Fig. 7.— *Top panel:* Integrated ^{12}CO (1–0) emission of the redshifted lobe of the outflow driven by the HH46/47 protostellar system based on the data presented by *Arce et al.* (2013), with the positions of three clump-like structures labeled. *Bottom panel:* Position-velocity diagram along the axis of the redshifted lobe of the same outflow. The three clumps clearly exhibit higher velocities than the rest of the outflowing gas, with each clump exhibiting its own Hubble law.

et al., 2010; *Schwarz et al.*, 2012). As discussed by *Dunham et al.* (2010b), the amount by which the accretion rates must have decreased over the lifetimes of the outflows are too large to be explained solely by the slowly declining accretion rates predicted by theories lacking short-timescale variability and bursts (see §3).

5.3. Chemical Signatures of Variable Accretion

If the accretion onto the central star is episodic, driving substantial changes in luminosity, there can be observable effects on the chemistry of the infalling envelope and these can provide clues to the luminosity history. Several authors have recently explored these effects using chemical evolution models, as discussed in more detail in the accompanying chapter on episodic accretion by *Audard et al.* A particular opportunity to trace the luminosity history exists in the absorption spectrum of CO_2 ice; observations of the 15.2 μm CO_2 ice absorption feature toward low-luminosity protostars with *Spitzer* spectroscopy have provided strong evidence for past accretion and luminosity bursts in these objects (*Kim et al.*, 2012, see §7).

6. THE FORMATION AND EVOLUTION OF PROTOSTELLAR DISKS

6.1. Theoretical Overview

The formation of a circumstellar disk is a key step in the formation of planets and/or binary star systems, where in this chapter "disk" refers to a rotationally supported, Keplerian structure. Disks must form readily during the star formation process as evidenced by their ubiquity during the T-Tauri phase (see Fig. 14 of *Hernández et al.*, 2007). In order to form a disk during the collapse phase, the infalling material must have some specific angular momentum (*Cassen and Moosman*, 1981); disks may initially start small and grow with time. The formation of the disk is not dependent on whether the angular momentum derives from initial cloud rotation (*Cassen and Moosman*, 1981; *Terebey et al.*, 1984) or the turbulent medium in which the core formed (e.g. *Offner et al.*, 2010), but the subsequent growth of the disk will depend on the distribution of angular momentum. After disk formation, most accreting material must be processed through the disk. Moreover, models for accretion bursts and outflows depend on the disk playing a dominant role (see §3 and the accompanying chapters by *Li et al.*, *Audard et al*, and *Frank et al.*). Finally, disk rotation, when detectable, allows the only means of direct determination of protostellar masses (see the accompanying chapter by *Dutrey et al.*), since spectral types are unavailable for most protostars that are too deeply embedded to detect with optical and/or near-infrared spectroscopy, and mass is only one of several parameters that determines the luminosity of a protostar (see §3.1).

Numerical hydrodynamic models of collapsing, rotating clouds predict the formation of massive and extended disks in the early embedded stages of protostellar evolution (*Vorobyov*, 2009a), with the disk mass increasing with the protostellar mass (*Vorobyov*, 2011b). However, these and earlier studies neglected the role of magnetic fields. *Allen et al.* (2003) presented ideal magneto-hydrodynamic (MHD) simulations examining the effects of magnetic braking and showed that collapsing material drags the magnetic field inward and increases the field strengths toward smaller radii. The magnetic field is anchored to the larger-scale envelope and molecular cloud, enabling angular momentum to be removed from the collapsing inner envelope, preventing the formation of a rotationally supported disk.

This finding is referred to as the "magnetic braking catastrophe" and had been verified in the ideal MHD limit analytically by *Galli et al.* (2006) and in further numerical simulations by *Mellon and Li* (2008). These studies concluded that the magnetic braking efficiency must be reduced in order to enable the formation of rotationally supported disks. Non-ideal MHD simulations have shown that Ohmic dissipation can enable the formation of only very small disks (R $\sim$10 $R_\odot$) that are not expected to grow to hundred-AU scales until after most of the envelope has dissipated in the Class II phase (*Dapp and Basu*, 2010; *Machida et al.*, 2011b). Disks with greater radial extent and larger masses can form if magnetic fields are both relatively weak and misaligned relative to the rotation axis (*Joos et al.*, 2012), and indeed observational evidence for such misalignments has been claimed by *Hull et al.* (2013). *Krumholz et al.* (2013) estimated that 10% - 50% of protostars might have large (R $>$ 100 AU), rotationally supported disks by applying current observational constraints on the strength and alignment of magnetic fields to the simulations of *Joos et al.*

(2012).

6.2. Observations of Protostellar Disks

The earliest evidence for the existence of protostellar disks comes from models fit to the unresolved infrared and (sub)millimeter continuum SEDs of protostars (e.g., *Adams and Shu*, 1986; *Kenyon et al.*, 1993; *Butner et al.*, 1994; *Calvet et al.*, 1997; *Whitney et al.*, 2003b; *Robitaille et al.*, 2006; *Young et al.*, 2004). Models including circumstellar disks provided good fits to the observed SEDs, and in many cases disks were required in order to obtain satisfactory fits. However, SED fitting is often highly degenerate between disk and inner core structure, and even in the best cases does not provide strong constraints on disk sizes and masses, the two most relevant quantities for evaluating the significance of magnetic braking. Thus in the following sections we concentrate on observations that do provide constraints on these quantities, with a particular focus on (sub)millimeter interferometric observations.

6.2.1. Class I Disks

Due to complications with separating disk and envelope emission, a characterization of Class I disks on par with Class II disks (e.g. *Andrews et al.*, 2010) has not yet been possible. Several approaches have been taken toward characterizing Class I disks, including focusing on SEDs, scattered light imaging, and millimeter emission.

Analysis of millimeter emission requires invoking models to disentangle disk and envelope emission. This approach was carried out by *Jorgensen et al.* (2009), who found 10 Class I disks with $M \sim 0.01$ M$_\odot$, although the disks were not resolved. *Eisner* (2012) modeled the disk and envelope properties of eight Class I protostars in Taurus combining the SEDs, millimeter imaging, and near-infrared scattered light imaging (see also *Eisner et al.*, 2005). The median radius of the sample was found to be 250 AU and the median disk mass was 0.01 $M_\odot$, but the derived parameters for each source depended strongly on the weighting of the model fits. They also did not resolve the disks, with only $\sim 1''$ resolution.

The most definitive constraints on Class I disks have come from the detailed modeling of edge-on disks resolved in both near-infrared scattered light and millimeter dust emission. Two recent examples of such work include studies of the edge-on Class I protostars IRAS 04302+2247 and CB26. IRAS 04302+2247 was found to have a disk with $R \sim 300$ AU and $M \sim 0.07$ M$_\odot$ (*Wolf et al.*, 2008; *Gräfe et al.*, 2013). CB26 has a disk with $R \sim 200$ AU and a possible inner hole of 45 AU cleared by an undetected binary companion (*Sauter et al.*, 2009). These representative cases illustrate that relatively large, massive disks may be common in the Class I stage.

Sensitive molecular line observations are also enabling the kinematic structure of Class I disks to be examined. A number of Class I disks have been found to be rotationally-supported (e.g. *Jorgensen et al.*, 2009; *Brinch et al.*, 2007; *Lommen et al.*, 2008; *Takakuwa et al.*, 2012; *Hara et al.*, 2013). Thus far, the number of Class I protostellar mass measurements is only 6, and their masses range between 0.37 and 2.5 $M_\odot$. The disk masses are typically less than 10% of the stellar masses, modulo uncertainties in calculating mass from dust emission and modeling systematics. *Jorgensen et al.* (2009) pointed out possible discrepancies between models of disk formation from the simple picture of an infalling, rotating envelope (*Terebey et al.*, 1984). Semi-analytic models of protostellar collapse from *Visser et al.* (2009) and hydrodynamic models of *Vorobyov* (2009a, 2011b) seem to suggest much more massive disks (up to 40%–60% that of the star) than revealed by observations.

6.2.2. Class 0 Disks

Observations of Class 0 disks face challenges similar to the Class I disks, but with the added complication of more massive envelopes responsible for $\sim$90% of the emission at millimeter wavelengths (*Looney et al.*, 2000). The SEDs of Class 0 protostars are dominated by the far-infrared component and the near-infrared is generally dominated by scattered light from the outflow cavity. Much like the Class I systems, it is impossible to garner any constraints of the disk properties in Class 0 systems from the SEDs alone.

B335 was one of the first Class 0 systems to be examined in great detail and found to have a disk with $R < 60$ AU and $M \sim 0.0014$ M$_\odot$ (*Harvey et al.*, 2003); while that study assumed a distance of 250 pc, we have scaled these numbers to the more recent estimates that place B335 at $\sim$150 pc (*Stutz et al.*, 2008). Among other Class 0 protostars, HH211 shows extended structure perpendicular to the outflow that may indicate a circumstellar disk (*Lee et al.*, 2009a). On the other hand, the Class 0 protostar L1157-mm shows no evidence of resolved disk structure on any scale with resolutions as fine as $0\farcs3$, implying any disk present must have $R < 40$ AU and $M < 0.004$–0.025 M$_\odot$ (*Chiang et al.*, 2012), and ALMA observations of IRAS 16293-2422 revealed only a very small disk with $R \sim 20$ AU. (*Chen et al.*, 2013; *Zapata et al.*, 2013). *Jørgensen et al.* (2007) and *Jorgensen et al.* (2009) coupled a submillimeter survey of 10 Class 0 protostars with models for envelope emission and found Class 0 disks with $M \sim 0.01$ M$_\odot$ (with significant scatter), and no evidence of disk mass growth between Class 0 and I sources. On the other hand, *Maury et al.* (2010) did not find any evidence for disk structures > 100 AU in a millimeter survey of 5 Class 0 protostars at sub-arcsecond resolution (linear resolution $<$100 AU).

The clearest evidence of Class 0 disks thus far is found toward the protostars L1527 IRS and VLA1623A. For L1527, high resolution scattered light and (sub)millimeter imaging observations found strong evidence of an edge-on disk, (*Tobin et al.*, 2012, see Fig. 8). Furthermore, molecular line observations were found to trace Keplerian rotation, implying a protostellar mass of 0.19 ± 0.04 M$_\odot$. The mass of the surrounding envelope is $\sim$5 times larger than the protostar, and the disk has $R = 70 - 125$ AU and $M \sim 0.007$

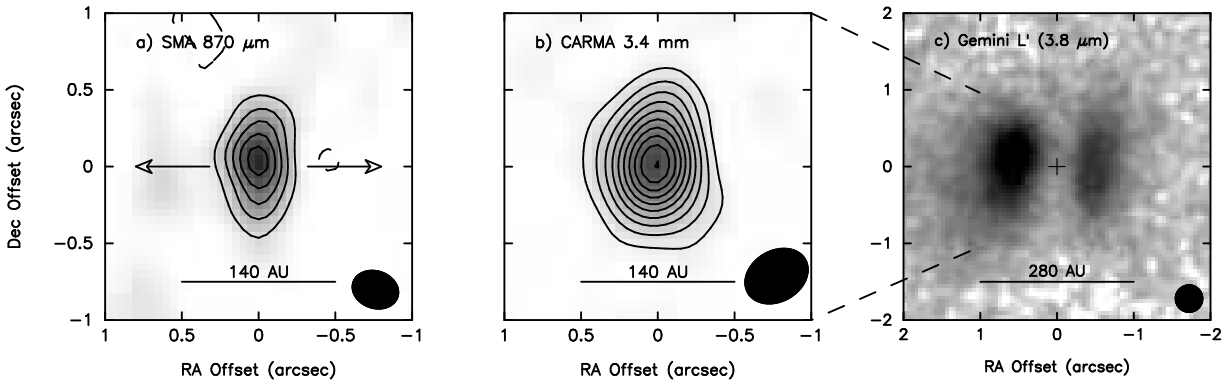

Fig. 8.— Images of the edge-on disk around the protostar L1527 from (*Tobin et al.*, 2012). High-resolution images of L1527 showing the disk in dust continuum emission and scattered light are shown at wavelengths of 870 μm from the SMA (a), 3.4 mm from CARMA (b), and 3.8 μm from Gemini (c). The Gemini image is shown on a larger scale. The sub/millimeter images are elongated in the direction of the dark lane shown in panel (c), consistent with an edge-on disk in this Class 0 protostellar system. The outflow direction is indicated by arrows in panel (a). The cross in panel (c) marks the central position of the disk from the SMA images.

$M_\odot$ (*Tobin et al.*, 2012, 2013). L1527 IRS is classified as Class 0 based on its SED. While its edge-on nature can bias this classification §2, it does have a more massive and extended envelope than a typical Class I protostar in Taurus and is consistent with the Stage 0 definition of $M_* < M_{env}$. For VLA1623A, *Murillo and Lai* (2013) and *Murillo et al.* (2013) identified a confirmed disk via detection of Keplerian rotation, with $R \sim 150$ and $M \sim 0.02$ $M_\odot$.

6.3. Summary of Protostellar Disks

Current observations clearly indicate that there are large (R $>$ 100 AU) disks present in the Class I phase but their properties have been difficult to detail en masse thus far. There is evidence for large disks in *some* Class 0 systems (L1527 IRS, VLA 1623, HH211), but more observations with sufficient resolution to probe scales where disks dominate the emission are needed for a broader characterization. Efforts to detect more disk structures in the nearby Perseus molecular cloud are underway and have found two strong candidates for Class 0 disks (*Tobin et al.*, in prep).

Despite remarkable progress in characterizing disks around protostars in the last decade, several puzzles remain. First, if disks form via a process similar to the rotating collapse model, the observed disk masses are about an order of magnitude lower than theoretical estimates for a given protostellar mass (*Vorobyov*, 2009a; *Visser et al.*, 2009; *Yorke and Bodenheimer*, 1999). Second, models considering magnetic braking seem to suggest small disks until the Class II phase, unless there are misaligned fields; however, observations seem to indicate at least some large disks in the Class 0 and I phases. Lastly, it is not clear if there is any observational evidence for magnetic braking during collapse, as *Yen et al.* (2013) recently showed that angular momentum is conserved in two Class 0 systems.

Moving forward, ALMA will provide key observations for determining the presence and properties of Class 0 disks, offering significant improvements over the resolution and sensitivity limits of current interferometers. By detecting Keplerian rotation, ALMA holds the promise to enable mass measurements for large numbers of protostars, possibly even directly observing for the first time the protostellar mass function (*McKee and Offner*, 2010). At the same time, the upgraded Very Large Array (VLA) has very high sensitivity to dust continuum emission at 7 mm and may also contribute to the characterization of protostellar disks.

7. THE EVOLUTION OF INFALLING MATERIAL

Silicate dust and ices are the building blocks of comets and, ultimately, Earth-like planets, and both undergo significant chemical and structural (crystallinity) changes during the protostellar stage. Understanding how these materials evolve as they flow from molecular cores to protostellar envelopes and disks is an essential component in determining how matter is modified in planet-forming disks. While most of this Chapter focuses on macroscopic protostellar evolution, we now examine the microscopic evolution of solid-state matter surrounding protostars.

Mid-infrared spectra toward low-mass protostars contain a wealth of solid-state absorption features due to the vibrational modes of silicate dust and many molecular ice species (e.g., *Boogert et al.*, 2008; *Furlan et al.*, 2008). These materials are inherited from the dense interstellar medium, and are present in the infalling envelopes and accretion disks surrounding protostars. Within such environments, radiative and mechanical processing by UV photons and accretion shocks may sublimate or modify the properties of dust and ices. Indeed, theoretical disk evolutionary models of low-mass protostars predict that infalling ices, with sublimation temperatures greater than $T \approx 50$ K, remain on grain surfaces after reaching the accretion disk (*Visser et al.*, 2009), suggesting that at least a fraction of cometary ices are of protostellar origin. Furthermore, the formation of crystalline silicates are predicted to have occurred during the earliest phases of disk formation, when a fraction of the amorphous silicate dust falls close to the central protostar

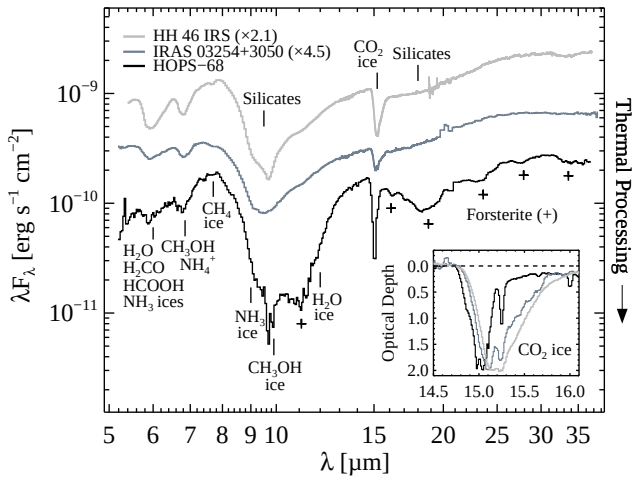

Fig. 9.— *Spitzer*-IRS spectra of low-mass prototstars, ordered by increasing evidence for thermal processing, with solid-state features indicated. Unlike HOPS 68 (black), the spectra of HH 46 IRS (gray) and IRAS 03254+3050 (dark gray) show no signs for the presence of crystalline silicates (forsterite). Insert: arbitrarily scaled CO_2 ice optical depth spectra of protostars, exhibiting various degrees of ice processing that is evident by their double-peaked substructure. Data are presented in *Boogert et al.* (2008); *Pontoppidan et al.* (2008); *Poteet et al.* (2011, 2013).

and is subsequently heated to temperatures of T = 800-1200 K (*Dullemond et al.*, 2006; *Visser and Dullemond*, 2010).

While it is generally assumed that solids present in the infallling envelopes of low-mass protostars are mostly pristine without significant processing, the *Spitzer Space Telescope* has now revealed that such matter shows clear evidence for thermal processing. In this section, we review the current observational evidence for high- to low-temperature processing of silicates and CO_2 ice, and their implications for both protostellar evolution and the inventory of matter delivered to planet-forming disks.

7.1. Thermal Processing of Amorphous Silicates

Prior to the launch of the *Spitzer Space Telescope*, little knowledge of the silicate dust surrounding low-mass protostars existed. Because observations with the *Infrared Space Observatory* were sensitivity-limited to the most luminous, massive protostars, detailed spectral modeling was possible for only a few high-mass protostars (*Demyk et al.*, 1999, 2000). Similar to the silicate composition of the diffuse interstellar medium, which is thought to be almost entirely amorphous in structure (*Kemper et al.*, 2005), only a small fraction (1%-2%) of the silicate dust mass present in protostellar envelopes was predicted to be in crystalline form during the pre-*Spitzer* era.

The high sensitivity of the Infrared Spectrograph (IRS) on board the *Spitzer Space Telescope* permitted the routine detection of crystalline silicates emission features toward T Tauri stars (e.g., *Sargent et al.*, 2009; *Olofsson et al.*, 2010) and comets (e.g., *Lisse et al.*, 2007; *Kelley and Wooden*, 2009). Crystalline silicate emission features are also detected toward the Serpens protostellar binary SVS 20 (*Ciardi et al.*, 2005); however, a recent evaluation of its *Spitzer*-IRS spectrum suggests that SVS 20 may be a T Tauri star possessing a flattened, settled disk (*Oliveira et al.*, 2010).

In contrast, more than 150 low-mass protostars have been studied in the literature, and their *Spitzer*-IRS spectra exhibit 10 and 20 μm amorphous silicate absorption features that are almost always characterized by broad, smooth profiles, lacking any superimposed narrow structure. However, the one exception is HOPS 68, a low-mass embedded protostar situated in the Orion Molecular Cloud complex (*Poteet et al.*, 2011). The *Spitzer*-IRS spectrum toward HOPS 68 exhibits narrow *absorption* features of forsterite (Fig. 9), indicating that a significant fraction ($\lesssim$17%) of amorphous silicates within its infalling envelope have experienced strong thermal processing ($T \gtrsim$ 1000 K). Although the mechanisms responsible for such processing are still not fully understood, it is proposed that amorphous silicates were annealed or vaporized within the warm inner region of the disk and/or envelope and subsequently transported outward by entrainment in protostellar outflows. Alternatively, an *in situ* formation by shock processing in the outflow working surface may be responsible for the production of crystalline silicates within the envelope of HOPS 68.

The detection of crystalline silicates in cometary material necessitates a process for transporting thermally processed silicates to the cold outer regions of planet-forming disks (e.g., *Ciesla*, 2011) or requires an *in situ* formation route to be present at large radial distances (e.g., *Vorobyov*, 2011a; *Nayakshin et al.*, 2011). The detection of crystalline silicates toward HOPS 68 demonstrates that at least in one case, thermally processed silicates may be delivered to the outer accretion disk by infall from the protostellar envelope. Of course, HOPS 68 may be a unique case. However, on the basis of its peculiar SED, it is argued that HOPS 68 has a highly flattened envelope structure that provides a line of sight to the inner region without passing through the intervening cold, outer envelope (*Poteet et al.*, 2011, 2013). Thus, HOPS 68 may provide a rare glimpse into the thermally processed inner regions of protostellar envelopes.

7.2. Thermal Processing of Interstellar CO_2 Ice

Interstellar ices serve as excellent tracers of the thermal history of protostellar environments (*Boogert and Ehrenfreund*, 2004). As material falls from the outer envelope to the accretion disk, grains are subject to elevated temperatures while traversing the inner envelope region, resulting in the crystallization of hydrogen-rich ices or the sublimation of CO-rich ices (e.g., *Visser et al.*, 2009). Moreover, protostellar feedback mechanisms, such as outflow-induced shocks and episodic accretion events, may also be responsible for the crystallization and sublimation of interstellar ices (*Bergin et al.*, 1998; *Lee*, 2007).

CO_2 ice has proven to be a sensitive diagnostic of the thermal history toward protostars. Pure CO_2 ice may be

produced by (1) segregation of CO_2 from hydrogen-rich ice mixtures (e.g., H_2O:CH_3OH:CO_2 and H_2O:CO_2) or (2) thermal desorption of CO from a CO:CO_2 ice mixture at temperatures of T = 30-60 K and T = 20-30 K, respectively (*Ehrenfreund et al.*, 1998; *Öberg et al.*, 2009; *van Broekhuizen et al.*, 2006). Spectroscopically, thermally processed mixtures of hydrogen- and CO-rich CO_2 ices produce a double-peaked substructure in the 15.2 μm CO_2 ice bending mode profile, characteristic of pure, crystalline CO_2 ice (Fig. 9).

The presence of pure CO_2 ice is generally interpreted as a result of thermal processing of pristine icy grains in cold, quiescent regions of dense molecular clouds. To date, $\sim$100 high-resolution *Spitzer*-IRS spectra toward low-mass protostars have been described in the literature, and the majority of the CO_2 is found in hydrogen- and CO-rich ices typical of molecular cloud cores (*Pontoppidan et al.*, 2008; *Zasowski et al.*, 2009; *Cook et al.*, 2011; *Kim et al.*, 2012). However, nearly 40% of the spectra show some evidence for the presence of pure CO_2 ice, suggesting that low-mass protostars have thermally processed inner envelopes. Among these, relatively large abundances ($\sim$15% of the total CO_2 ice column density) of pure CO_2 ice have been detected toward a sample of low-luminosity (0.08 $L_\odot \lesssim L \lesssim$ 0.69 $L_\odot$) embedded protostars (*Kim et al.*, 2012). Because the present environments of low-luminosity protostars do not provide the thermal conditions needed to produce pure CO_2 in their inner envelopes, a transient phase of higher luminosity must have existed some time in the past (*Kim et al.*, 2012). The presence and abundance of pure CO_2 ice toward these low-luminosity protostars may be explained by episodic accretion events, in which pure CO_2 is produced by distillation of a CO:CO_2 mixture during each high-luminosity transient phase. Other accretion models have not yet been tested and may also explain the observed presence of pure CO_2 ice toward low-luminosity protostars; however, continuous accretion models with monotonically increasing luminosity cannot reproduce the observed abundances of CO_2 ice and $C^{18}O$ gas (*Kim et al.*, 2012).

The highest level of thermally processed CO_2 ice is found toward the moderately luminous (1.3 $L_\odot$) protostar HOPS 68 (*Poteet et al.*, 2013). Its CO_2 ice spectrum reveals an anomalous 15.2 μm bending mode profile that indicates little evidence for the presence of unprocessed ice. Detailed profile analysis suggests that 87%-92% of its CO_2 ice is sequestered as spherical, CO_2-rich mantles, while typical interstellar ices are dominated by irregularly shaped, hydrogen-rich CO_2 mantles (e.g., *Pontoppidan et al.*, 2008). The nearly complete absence of unprocessed ices along the line of sight to HOPS 68 is best explained by a highly flattened envelope structure, which lacks cold absorbing material in its outer envelope, and possesses a large fraction of material within its inner (10 AU) envelope region. Moreover, it is proposed that the spherical, CO_2-rich ice mantles formed as volatiles rapidly froze out in dense gas, following an energetic but transient event that sublimated primordial ices within the inner envelope region of HOPS 68. The mechanism responsible for the sublimation is proposed to be either an episodic accretion event or shocks in the interaction region between the protostellar outflow and inner envelope. Presently, it is unknown if such feedback mechanisms are also responsible for the presence of crystalline silicates toward HOPS 68.

8. DOES ENVIRONMENT MATTER?

Low mass stars form in a wide range of environments: isolated globules, small groups, and rich clusters of low and high mass stars (e.g. *Gutermuth et al.*, 2009; *Launhardt et al.*, 2013), with no apparent dichotomy between clustered and isolated star formation (*Bressert et al.*, 2010). This range of environments provides a natural laboratory for studying low mass star formation in different physical conditions, with the goal of elucidating how those physical conditions may guide the formation of the stars. In this section, we explore how the environment affects the incidence of protostars and their properties. We define local environment as the region outside the immediate core/envelope, i.e. beyond 10,000-20,000 AU (*Enoch et al.*, 2008). Thus, the environmental conditions would include the properties of the gas in the surrounding molecular cloud or the density of young stars in the vicinity of the protostar, but would exclude the local molecular core/envelope as well as companions in a multiple star system.

Many of the environmental conditions have yet to be measured over the spatial extent of the *Spitzer* and *Herschel* surveys. Thus we focus on three measures of the environment: the gas column density, cloud geometry, and the surface density of YSOs, to address four specific questions.

8.1. Does the Incidence and Density of Protostars Depend on the Local Gas Column Density?

A combination of (sub)millimeter surveys for cores and extinction maps constructed from 2MASS and *Spitzer* photometry of background stars have enabled an examination of the incidence of molecular cores as a function of the column density of gas smoothed over spatial scales of 0.2 to 1 pc (see also the accompanying chapter by *Padoan et al.* for a similar discussion in the context of star formation laws). Millimeter continuum surveys of the Ophiuchus and Serpens clouds show that the cores are found in environments where the column densities exceed $A_V = 7$ mag (*Johnstone et al.*, 2004; *Enoch et al.*, 2008), consistent with the model of photoionization regulated star formation in magnetized clouds (*McKee*, 1989). However, in the Perseus cloud, *Enoch et al.* (2008) found that 25% of cores are located at $A_V < 7$ mag (however, see *Kirk et al.*, 2006), and *Hatchell et al.* (2005) showed that the probability of finding a sub-millimeter core in the Perseus cloud increased continuously with the integrated intensity of the $C^{18}O$ ($1 \rightarrow 0$) line to the 3rd power. In total, these results indicate a rapid rise in the incidence of cores with column density, but with a small number of cores detected below $A_V = 7$ mag.

A similar result comes from the examination of *Spitzer*

identified infrared protostars. In a combined sample of seven molecular clouds, *Gutermuth et al.* (2011) and *Masiunas et al.* (2012) showed that the surface density of dusty YSOs (i.e. Class 0/I *and* Class II objects) increases with the 2nd to 3rd power of the gas column density. *Heiderman et al.* (2010) also found a steep rise in the surface density of c2d and GB protostars with the column density of gas. Although *Spitzer* identified candidate protostars at column densities as low as 60 $M_\odot$ pc^{-2} ($A_V = 3$ mag, *Gutermuth et al.*, 2011), the protostars are preferentially found in much denser environments, with a rapid, power-law like rise in the density of protostars with increasing gas column density. Currently, it is not clear whether the rapid rise in the incidence of cores and density of protostars with column density is due to the inhibition of star formation in regions of low column density, as argued by the photoionization regulated star formation model, or a non-linear dependence of the density of protostars on the gas column density, such as that predicted by Jeans fragmentation (*Larson*, 1985).

8.2. What is the Connection between Cloud Geometry and the Spatial Distribution of Protostars?

The elongated and filamentary nature of interstellar clouds has been evident since the earliest optical observations of dark clouds (*Barnard*, 1907). With improvements in sensitivity and resolution, it has become clear that star-forming molecular clouds are complex filamentary networks, with filamentary structure on scales from hundreds of pc to hundreds of AU (*Lynds*, 1962; *Schneider and Elmegreen*, 1979; *Myers*, 2009a; *Tobin et al.*, 2010; *André et al.*, 2010; *Molinari et al.*, 2010). Large-scale filaments harbor star-forming cores and protostars, especially at bends, branch points, or hubs which host groups or clusters of cores and protostars (*Myers*, 2009a; *Schneider et al.*, 2012). Filaments may both accrete gas and channel its flow along their length (*Csengeri et al.*, 2011); recent observations of one young cluster found that flow onto and along filaments may feed gas to the central, cluster-forming hub (*Kirk et al.*, 2013). The filamentary structure of star-forming gas in Orion and the corresponding distribution of protostars is apparent in Fig. 10.

Self-gravitating filaments may fragment with a characteristic spacing (*Larson*, 1985; *Inutsuka and Miyama*, 1992, 1997). Indeed, the spacings determined from the initial temperature, surface density, and length of observed filaments predict the approximate number of low-mass stars in the Taurus complex and other complexes which lack rich clusters (*Hartmann*, 2002; *Myers*, 2011). A relationship between the spacing of protostars with gas column density is clearly apparent in Fig. 10, which shows recent HOPS observations of two filamentary regions within the Orion cloud. The OMC-2/3 region is directly north of the Orion Nebula and is considered a northern extension of the ONC (*Peterson and Megeath*, 2008; *Megeath et al.*, 2012). In contrast, L1641S is a more quiescent region in the southern part of the L1641 cloud (*Carpenter*, 2000; *Allen and Davis*, 2008). Although both regions host multi-parsec filaments with mass to length ratios exceeding the limit for a stable, thermally supported filament (*André et al.*, 2010; *Fischera and Martin*, 2012), the average column density calculated above a cutoff of $N(H_2) = 3 \times 10^{21}$ cm^{-2} is twice as high in OMC2/3: $N(H_2) = 1.4 \times 10^{22}$ cm^{-2} in OMC2/3 as compared to 7.6×10^{21} cm^{-2} in L1641S. The density of protostars is correspondingly higher in the OMC2/3 region; with the typical protostellar spacing being 6500 AU and 14000 AU in OMC2/3 and L1641, respectively.

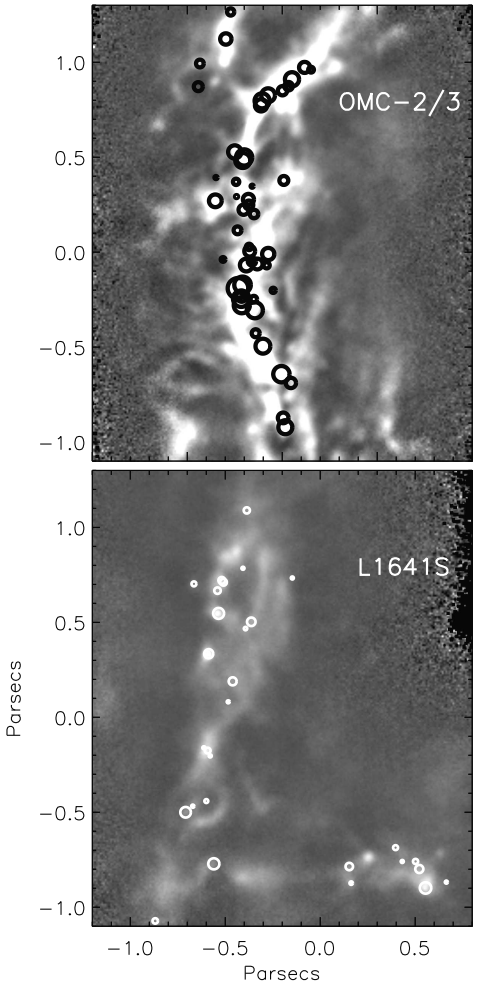

Fig. 10.— APEX/LABOCA 870 μm maps of two regions in the Orion molecular clouds: OMC-2/3 and L1641S (Stanke et al., in prep.). They are plotted on the same spatial scale with the same intensity scale for the 870 μm intensity. Overlaid are the position of the protostars; the size of the symbol is proportional to the log of the luminosity determined from the HOPS data.

8.3. What Fraction of Protostars May be Interacting?

With most protostars concentrated in regions of high gas column density and high stellar surface density, interactions between protostars may be common. *Winston et al.* (2007) found that the protostars in the Serpens main cluster have a

median projected separation of 8000 AU (corrected to the revised distance for Serpens of 429 pc (*Dzib et al.*, 2011)); smaller than the typical diameter of cores of 10,000-20,000 AU (*Enoch et al.*, 2008). They also found that the low relative velocities of the protostars and high gas density of the surrounding cloud core are consistent with the competitive accretion models of *Bonnell and Bate* (2006), where the protostars compete for gas from a common reservoir. The projected spacing of the protostars in OMC2/3 is also smaller than the typical diameters of cores (Fig. 10, also see *Takahashi et al.*, 2013; *Li et al.*, 2013). *Megeath et al.* (in prep.) examined the spacing between the *Spitzer* identified protostars in the Orion molecular clouds. They found that 11% and 23% of the protostars are within a projected separation of 5000 and 10,000 AU from another protostar, respectively. Thus, sources separated by $\leq 10,000$ AU would potentially be able to interact through the collisions of their envelopes and tidal forces. However, since the actual separations are larger than the measured projected separations, these percentages should be considered upper limits. On the other hand, dynamical motions in such highly clustered regions (e.g., *Parker and Meyer*, 2012) may increase the percentage of sources that interact.

8.4. Do the Properties of Protostars Depend on their Environment?

In their study of the protostellar luminosity distributions (hereafter: PLDs) in nine nearby molecular clouds, *Kryukova et al.* (2012) searched for variations between the high and low density environments within a single cloud. By dividing protostars into two samples based on the local surface density of YSOs, they compared PLDs for protostars located in crowded, high density regions to those in regions of low densities. In the Orion molecular clouds, they found the PLDs of the high and low stellar density regions had a very low probability of being drawn from the same parent distribution, with the PLD for the protostars in denser environments biased to higher luminosities. Thus, within the Orion molecular clouds, the luminosities of the protostars appears to depend on the surface density of the YSOs in the surrounding environment. Unfortunately, the smaller numbers of protostars found in the other eight molecular clouds precluded a definitive comparison of the high and low density regions in those clouds.

One weakness of the Kryukova et al. study is the use of an empirical relationship to extrapolate from the infrared to bolometric luminosity. However, using the full SEDs from HOPS (Fig. 1) to directly determine the bolometric luminosity of the protostars in Fig. 10; the median L_{bol} is 6.2 $L_{\odot}$ in the densely clustered OMC2/3 region and 0.7 $L_{\odot}$ in lower density L1641S region. This corroborates the result of *Kryukova et al.* (2012) by showing the more densely clustered OMC2/3 region has systematically higher luminosity protostars. Furthermore, it supports an interconnected relationship between the column density of the gas, the luminosities of the protostars, and the surface density of the protostars: filaments with higher gas column density will have both a higher density of protostars and more luminous protostars. In the near future, *Herschel* and ground-based (sub)millimeter imaging of protostellar environments should revolutionize our understanding of how the properties of protostars depend on their environment, and thereby place strong constraints on models of protostellar evolution.

9. SUMMARY

We have reported on recent progress in finding, identifying, and characterizing protostars in nearby clouds using infrared surveys and follow-up studies. The coverage, sensitivity, and resolution of *Spitzer* and *Herschel* have revealed objects of very low ($L_{\rm int} < 0.1$ L$_{\odot}$) luminosity (VeLLOs), objects with very red SEDS (PBRS), and candidates for first hydrostatic cores (FHSCs). Based on the full census of YSOs found in the c2d, Gould Belt, Orion, and Taurus surveys, classified as in *Greene et al.* (1994), and an assumed lifetime for Class II objects of 2 Myr, we infer Class 0+I lifetimes of 0.42 to 0.54 Myr, with the longer estimate applying to the Gould Belt clouds. While some differences in identification and classification remain, we have attempted to minimize them.

The luminosity distribution is very broad. After reviewing models of evolution, focusing on the accretion histories, we compared the luminosity distributions from the models to the observations; either mass dependent or episodic accretion models can match the data, but the isothermal sphere, constant accretion rate, model cannot. Evidence of protostellar luminosity variability, outflow episodicity, and ice evolution all support some form of episodic accretion. The remaining questions are how extreme the variations can be, what the effect of variations are, and how much of the mass of the protostar is accreted during episodes of high accretion. Challenges for the future are to constrain short-term (decade scale) variability as a possible clue to longer term (e.g., 10^3 yr) variability, and to ultimately determine the relative importance of stochastic (episodic) and secular processes in building the final masses of stars.

The first stage of star formation, the first hydrostatic core, remains elusive. There are a number of candidates, but more theoretical work is needed to pin down the expected characteristics and to understand the evolutionary status of the other novel objects, such as PBRS and VeLLOs.

The existence and properties of disks in the protostellar phase are beginning to yield to observational scrutiny, and ALMA will provide a major advance. Current evidence suggests early formation of relatively massive disks, although only a small number of detections have been made to date. Theories without magnetic fields predict more massive disks than seen, while theories with rotation axes and magnetic fields aligned struggle to create disks at all. Further theoretical exploration is needed to understand the relationship of mass infall rate from the core, its transition to the disk, and the processes that allow it to accrete onto the growing star. Typical Stage II disks process matter about

100 times more slowly than matter falls in during Stage I, so faster processes are needed in Stage I to avoid mass build-up and instabilities.

Material falling onto the disk undergoes substantial chemical and, in some cases, mineralogical evolution. Dust grains grow and may become crystallized, while ice in mantles evolves chemically. Distillation of pure CO_2 ice provides clues to the luminosity evolution. The state of ice and gas arriving at the disk set the stage for later chemical evolution during Stage II.

The complete surveys reported here reveal the location of star formation within molecular clouds. Prestellar cores and protostars are highly concentrated in regions of high surface, and presumably volume, density (see the accompanying chapter by *Padoan et al.*). The protostars in the very crowded environments of Orion appear to be systematically more luminous, and may be interacting in the regions of highest protostellar density. The "clumps" hosting cluster formation are generally very filamentary, and rich clusters prefer the nexus of filaments for their maternity wards.

The future is bright. ALMA will allow studies of unprecedented detail of the density, temperature, and velocity fields in infalling envelopes (e.g., *Pineda et al.*, 2012). Studies of embedded disks will clarify their masses and sizes, and detection of Keplerian motions will finally constrain the masses of the growing stars. JWST will allow deeper studies of the shorter (infrared) wavelenths of deeply embedded objects, and SOFIA will provide spectroscopic data on the brighter sources. On the theoretical side, modelers should use physically realistic calculations to predict self-consistently all the observations: the IMF and its realization in different regions, the structure, velocity field, and chemistry of infalling envelopes, the luminosity distribution, protostellar disk sizes and masses, the diversity of disks emerging in the Stage II phase, variability measurements, protostellar masses (measured with Keplerian disks with ALMA and NOEMA, the successor to the PdBI), and environmental dependencies.

Acknowledgments. The authors thank R. Launhardt, J. Green, and H. G. Arce for providing data for Fig. 1 and Fig. 7, and the anonymous referee for comments that have improved this review. This review is based primarily on observations made with the *Spitzer Space Telescope* and *Herschel Space Observatory*. *Spitzer* is operated by the Jet Propulsion Laboratory, California Institute of Technology under a contract with NASA, and *Herschel* is an ESA space observatory with science instruments provided by European-led Principal Investigator consortia and with important participation from NASA. This review has made use of NASA's Astrophysics Data System Bibliographic Services. MMD, STM and WJF acknowledge support from NASA through awards issued by JPL/Caltech, and MMD acknowledges NSF support through grant AST-0845619 to Yale University. The work of AMS was supported by the Deutsche Forschungsgemeinschaft priority program 1573 ("Physics of the Interstellar Medium"). NJE acknowledges support from the NSF through grant AST-1109116 to the University of Texas at Austin. CAP acknowledges support provided by the NASA Astrobiology Institute through contract NNA09DA80A. JT acknowledges support provided by NASA through Hubble Fellowship grant #HST-HF-51300.01-A awarded by the Space Telescope Science Institute, which is operated by the Association of Universities for Research in Astronomy, Inc., for NASA, under contract NAS 5-26555. EIV performed numerical simulations on the SHARCNET, ACEnet, VSC-2 scientific computer clusters, and acknowledges support from RFBR grant 13-02-00939.

REFERENCES

Adams F. C. and Shu F. H. (1986) *Astrophys. J.*, *308*, 836.
Adams F. C. and Shu F. H. (2007) *Astrophys. J.*, *671*, 497.
Adams F. C. et al. (1987) *Astrophys. J.*, *312*, 788.
Aikawa Y. et al. (2012) *Astrophys. J.*, *760*, 40.
Ali B. et al. (2010) *Astron. Astrophys.*, *518*, L119.
Allen A. et al. (2003) *Astrophys. J.*, *599*, 363.
Allen L. et al. (2007) *Protostars and Planets V*, pp. 361–376.
Allen L. E. and Davis C. J. (2008) *Low Mass Star Formation in the Lynds 1641 Molecular Cloud*, p. 621.
Andre P. et al. (1993) *Astrophys. J.*, *406*, 122.
André P. et al. (2010) *Astron. Astrophys.*, *518*, L102.
Andrews S. M. et al. (2010) *Astrophys. J.*, *723*, 1241.
Arce H. G. and Goodman A. A. (2001) *Astrophys. J.*, *554*, 132.
Arce H. G. et al. (2013) *ArXiv e-prints*.
Armitage P. J. (2011) *Annu. Rev. Astron. Astrophys.*, *49*, 195.
Audard M. et al. (2007) *Astron. Astrophys.*, *468*, 379.
Bachiller R. et al. (1991) *Astron. Astrophys.*, *251*, 639.
Balbus S. A. and Hawley J. F. (1991) *Astrophys. J.*, *376*, 214.
Baraffe I. et al. (2009) *Astrophys. J. Lett.*, *702*, L27.
Baraffe I. et al. (2012) *Astrophys. J.*, *756*, 118.
Barnard E. E. (1907) *Astrophys. J.*, *25*, 218.
Barnes P. J. et al. (2011) *Astrophys. J. Suppl.*, *196*, 12.
Baruteau C. et al. (2011) *Mon. Not. R. Astron. Soc.*, *416*, 1971.
Basu S. and Jones C. E. (2004) *Mon. Not. R. Astron. Soc.*, *347*, L47.
Bate M. R. (2011) *Mon. Not. R. Astron. Soc.*, *417*, 2036.
Bate M. R. and Bonnell I. A. (2005) *Mon. Not. R. Astron. Soc.*, *356*, 1201.
Belloche A. et al. (2006) *Astron. Astrophys.*, *454*, L51.
Bergin E. A. and Tafalla M. (2007) *Annu. Rev. Astron. Astrophys.*, *45*, 339.
Bergin E. A. et al. (1998) *Astrophys. J.*, *499*, 777.
Billot N. et al. (2012) *Astrophys. J. Lett.*, *753*, L35.
Blaes O. M. and Balbus S. A. (1994) *Astrophys. J.*, *421*, 163.
Bonnell I. A. and Bate M. R. (2006) *Mon. Not. R. Astron. Soc.*, *370*, 488.
Bonnell I. A. et al. (2001) *Mon. Not. R. Astron. Soc.*, *323*, 785.
Boogert A. C. A. and Ehrenfreund P. (2004) in: *Astrophysics of Dust*, vol. 309 of *Astronomical Society of the Pacific Conference Series*, (edited by A. N. Witt, G. C. Clayton, and B. T. Draine), p. 547.
Boogert A. C. A. et al. (2008) *Astrophys. J.*, *678*, 985.
Boss A. P. and Yorke H. W. (1995) *Astrophys. J. Lett.*, *439*, L55.
Bourke T. L. et al. (2006) *Astrophys. J. Lett.*, *649*, L37.
Bressert E. et al. (2010) *Mon. Not. R. Astron. Soc.*, *409*, L54.
Brinch C. et al. (2007) *Astron. Astrophys.*, *461*, 1037.
Brinch C. et al. (2009) *Astron. Astrophys.*, *502*, 199.
Butner H. M. et al. (1994) *Astrophys. J.*, *420*, 326.
Calvet N. et al. (1994) *Astrophys. J.*, *434*, 330.

Calvet N. et al. (1997) *Astrophys. J.*, *481*, 912.
Carpenter J. M. (2000) *Astron. J.*, *120*, 3139.
Carpenter J. M. et al. (2001) *Astron. J.*, *121*, 3160.
Carpenter J. M. et al. (2002) *Astron. J.*, *124*, 1001.
Cassen P. and Moosman A. (1981) *Icarus*, *48*, 353.
Cha S.-H. and Nayakshin S. (2011) *Mon. Not. R. Astron. Soc.*, *415*, 3319.
Chen H. et al. (1995) *Astrophys. J.*, *445*, 377.
Chen X. et al. (2010) *Astrophys. J.*, *715*, 1344.
Chen X. et al. (2012) *Astrophys. J.*, *751*, 89.
Chen X. et al. (2013) *Astrophys. J.*, *768*, 110.
Chiang H.-F. et al. (2012) *Astrophys. J.*, *756*, 168.
Ciardi D. R. et al. (2005) *Astrophys. J.*, *629*, 897.
Ciesla F. J. (2011) *Astrophys. J.*, *740*, 9.
Commerçon B. et al. (2012a) *Astron. Astrophys.*, *545*, A98.
Commerçon B. et al. (2012b) *Astron. Astrophys.*, *548*, A39.
Cook A. M. et al. (2011) *Astrophys. J.*, *730*, 124.
Crapsi A. et al. (2008) *Astron. Astrophys.*, *486*, 245.
Csengeri T. et al. (2011) *Astrophys. J. Lett.*, *740*, L5.
Dapp W. B. and Basu S. (2010) *Astron. Astrophys.*, *521*, L56.
Demyk K. et al. (1999) *Astron. Astrophys.*, *349*, 267.
Demyk K. et al. (2000) in: *ISO Beyond the Peaks: The 2nd ISO Workshop on Analytical Spectroscopy*, vol. 456 of *ESA Special Publication*, (edited by A. Salama, M. F. Kessler, K. Leech, and B. Schulz), p. 183.
di Francesco J. et al. (2007) *Protostars and Planets V*, pp. 17–32.
Dullemond C. P. et al. (2006) *Astrophys. J. Lett.*, *640*, L67.
Dunham M. M. and Vorobyov E. I. (2012) *Astrophys. J.*, *747*, 52.
Dunham M. M. et al. (2006) *Astrophys. J.*, *651*, 945.
Dunham M. M. et al. (2008) *Astrophys. J. Suppl.*, *179*, 249.
Dunham M. M. et al. (2010a) *Astrophys. J.*, *710*, 470.
Dunham M. M. et al. (2010b) *Astrophys. J.*, *721*, 995.
Dunham M. M. et al. (2013) *Astron. J.*, *145*, 94.
Dzib S. et al. (2011) in: *Revista Mexicana de Astronomia y Astrofisica Conference Series*, vol. 40 of *Revista Mexicana de Astronomia y Astrofisica Conference Series*, pp. 231–232.
Ehrenfreund P. et al. (1998) *Astron. Astrophys.*, *339*, L17.
Eisner J. A. (2012) *Astrophys. J.*, *755*, 23.
Eisner J. A. et al. (2005) *Astrophys. J.*, *635*, 396.
Enoch M. L. et al. (2008) *Astrophys. J.*, *684*, 1240.
Enoch M. L. et al. (2009) *Astrophys. J.*, *692*, 973.
Enoch M. L. et al. (2010) *Astrophys. J. Lett.*, *722*, L33.
Evans II N. J. et al. (2003) *PASP*, *115*, 965.
Evans II N. J. et al. (2009) *Astrophys. J. Suppl.*, *181*, 321.
Fatuzzo M. et al. (2004) *Astrophys. J.*, *615*, 813.
Findeisen K. et al. (2013) *Astrophys. J.*, *768*, 93.
Fischer W. J. et al. (2010) *Astron. Astrophys.*, *518*, L122.
Fischer W. J. et al. (2012) *Astrophys. J.*, *756*, 99.
Fischer W. J. et al. (2013) *Astronomische Nachrichten*, *334*, 53.
Fischera J. and Martin P. G. (2012) *Astron. Astrophys.*, *542*, A77.
Flaherty K. M. et al. (2012) *Astrophys. J.*, *748*, 71.
Flaherty K. M. et al. (2013) *Astron. J.*, *145*, 66.
Furlan E. et al. (2008) *Astrophys. J. Suppl.*, *176*, 184.
Galli D. et al. (2006) *Astrophys. J.*, *647*, 374.
Gammie C. F. (1996) *Astrophys. J.*, *457*, 355.
Gräfe C. et al. (2013) *Astron. Astrophys.*, *553*, A69.
Green J. D. et al. (2013a) *ArXiv e-prints*.
Green J. D. et al. (2013b) *Astrophys. J.*, *770*, 123.
Greene T. P. et al. (1994) *Astrophys. J.*, *434*, 614.
Gutermuth R. A. et al. (2009) *Astrophys. J. Suppl.*, *184*, 18.
Gutermuth R. A. et al. (2011) *Astrophys. J.*, *739*, 84.
Hara C. et al. (2013) *ArXiv e-prints*.
Hartmann L. (2002) *Astrophys. J.*, *578*, 914.
Harvey D. W. A. et al. (2003) *Astrophys. J.*, *596*, 383.
Harvey P. et al. (2007) *Astrophys. J.*, *663*, 1149.
Hatchell J. et al. (2005) *Astron. Astrophys.*, *440*, 151.
Heiderman A. et al. (2010) *Astrophys. J.*, *723*, 1019.
Herbig G. H. (1952) *JRASC*, *46*, 222.
Hernández J. et al. (2007) *Astrophys. J.*, *662*, 1067.
Hosokawa T. et al. (2011) *Astrophys. J.*, *738*, 140.
Hsieh T.-H. and Lai S.-P. (2013) *Astrophys. J. Suppl.*, *205*, 5.
Hull C. L. H. et al. (2013) *Astrophys. J.*, *768*, 159.
Inutsuka S.-I. and Miyama S. M. (1992) *Astrophys. J.*, *388*, 392.
Inutsuka S.-I. and Miyama S. M. (1997) *Astrophys. J.*, *480*, 681.
Johnstone D. et al. (2004) *Astrophys. J. Lett.*, *611*, L45.
Johnstone D. et al. (2013) *Astrophys. J.*, *765*, 133.
Joos M. et al. (2012) *Astron. Astrophys.*, *543*, A128.
Jørgensen J. K. et al. (2007) *Astrophys. J.*, *659*, 479.
Jorgensen J. K. et al. (2009) *Astron. Astrophys.*, *507*, 861.
Joy A. H. (1945) *Astrophys. J.*, *102*, 168.
Kauffmann J. et al. (2011) *Mon. Not. R. Astron. Soc.*, *416*, 2341.
Kelley M. S. and Wooden D. H. (2009) *Planet. Space Sci.*, *57*, 1133.
Kemper F. et al. (2005) *Astrophys. J.*, *633*, 534.
Kenyon S. J. and Hartmann L. (1995) *Astrophys. J. Suppl.*, *101*, 117.
Kenyon S. J. et al. (1990) *Astron. J.*, *99*, 869.
Kenyon S. J. et al. (1993) *Astrophys. J.*, *414*, 676.
Kim H. J. et al. (2012) *Astrophys. J.*, *758*, 38.
Kirk H. et al. (2006) *Astrophys. J.*, *646*, 1009.
Kirk H. et al. (2013) *Astrophys. J.*, *766*, 115.
Kóspál Á. et al. (2012) *Astrophys. J. Suppl.*, *201*, 11.
Kratter K. M. et al. (2008) *Astrophys. J.*, *681*, 375.
Kratter K. M. et al. (2010a) *Astrophys. J.*, *708*, 1585.
Kratter K. M. et al. (2010b) *Astrophys. J.*, *710*, 1375.
Krumholz M. R. et al. (2012) *Astrophys. J.*, *754*, 71.
Krumholz M. R. et al. (2013) *Astrophys. J. Lett.*, *767*, L11.
Kryukova E. et al. (2012) *Astron. J.*, *144*, 31.
Lada C. J. (1987) in: *Star Forming Regions*, vol. 115 of *IAU Symposium*, (edited by M. Peimbert and J. Jugaku), pp. 1–17.
Larson R. B. (1969) *Mon. Not. R. Astron. Soc.*, *145*, 271.
Larson R. B. (1985) *Mon. Not. R. Astron. Soc.*, *214*, 379.
Laughlin G. and Bodenheimer P. (1994) *Astrophys. J.*, *436*, 335.
Launhardt R. et al. (2013) *Astron. Astrophys.*, *551*, A98.
Lee C.-F. et al. (2009a) *Astrophys. J.*, *699*, 1584.
Lee C. W. et al. (2009b) *Astrophys. J.*, *693*, 1290.
Lee J.-E. (2007) *Journal of Korean Astronomical Society*, *40*, 83.
Lee J.-E. et al. (2010) *Astrophys. J. Lett.*, *709*, L74.
Li D. et al. (2013) *Astrophys. J. Lett.*, *768*, L5.
Lin D. N. C. and Pringle J. E. (1987) *Mon. Not. R. Astron. Soc.*, *225*, 607.
Lisse C. M. et al. (2007) *Icarus*, *191*, 223.
Lodato G. and Rice W. K. M. (2004) *Mon. Not. R. Astron. Soc.*, *351*, 630.
Lommen D. et al. (2008) *Astron. Astrophys.*, *481*, 141.
Looney L. W. et al. (2000) *Astrophys. J.*, *529*, 477.
Lynds B. T. (1962) *Astrophys. J. Suppl.*, *7*, 1.
Machida M. et al. (2011a) *Astrophys. J.*, *729*, 42.
Machida M. N. and Matsumoto T. (2011) *Mon. Not. R. Astron. Soc.*, *413*, 2767.
Machida M. N. et al. (2008) *Astrophys. J.*, *676*, 1088.
Machida M. N. et al. (2011b) *PASJ*, *63*, 555.
Manoj P. et al. (2013) *Astrophys. J.*, *763*, 83.
Martin R. G. et al. (2012) *Mon. Not. R. Astron. Soc.*, *423*, 2718.

Masiunas L. C. et al. (2012) *Astrophys. J.*, *752*, 127.
Masunaga H. et al. (1998) *Astrophys. J.*, *495*, 346.
Maury A. J. et al. (2010) *Astron. Astrophys.*, *512*, A40.
McKee C. F. (1989) *Astrophys. J.*, *345*, 782.
McKee C. F. and Offner S. S. R. (2010) *Astrophys. J.*, *716*, 167.
McKee C. F. and Tan J. C. (2003) *Astrophys. J.*, *585*, 850.
Megeath S. T. et al. (2009) *Astron. J.*, *137*, 4072.
Megeath S. T. et al. (2012) *Astron. J.*, *144*, 192.
Mellon R. R. and Li Z.-Y. (2008) *Astrophys. J.*, *681*, 1356.
Molinari S. et al. (2010) *Astron. Astrophys.*, *518*, L100.
Morales-Calderón M. et al. (2011) *Astrophys. J.*, *733*, 50.
Mottram J. C. et al. (2013) *Astron. Astrophys.*, *558*, A126.
Murillo N. M. and Lai S.-P. (2013) *Astrophys. J. Lett.*, *764*, L15.
Murillo N. M. et al. (2013) *ArXiv e-prints*.
Muzerolle J. et al. (1998) *Astron. J.*, *116*, 2965.
Myers P. C. (2009a) *Astrophys. J.*, *700*, 1609.
Myers P. C. (2009b) *Astrophys. J.*, *706*, 1341.
Myers P. C. (2010) *Astrophys. J.*, *714*, 1280.
Myers P. C. (2011) *Astrophys. J.*, *735*, 82.
Myers P. C. (2012) *Astrophys. J.*, *752*, 9.
Myers P. C. and Ladd E. F. (1993) *Astrophys. J. Lett.*, *413*, L47.
Nayakshin S. et al. (2011) *Mon. Not. R. Astron. Soc.*, *416*, L50.
Norman C. and Silk J. (1980) *Astrophys. J.*, *238*, 158.
Öberg K. I. et al. (2009) *Astron. Astrophys.*, *505*, 183.
Offner S. S. R. and McKee C. F. (2011) *Astrophys. J.*, *736*, 53.
Offner S. S. R. et al. (2009) *Astrophys. J.*, *703*, 131.
Offner S. S. R. et al. (2010) *Astrophys. J.*, *725*, 1485.
Offner S. S. R. et al. (2011) *Astrophys. J.*, *743*, 91.
Oliveira I. et al. (2010) *Astrophys. J.*, *714*, 778.
Olofsson J. et al. (2010) *Astron. Astrophys.*, *520*, A39.
Omukai K. (2007) *PASJ*, *59*, 589.
Ostriker E. C. and Shu F. H. (1995) *Astrophys. J.*, *447*, 813.
Palla F. and Stahler S. W. (1992) *Astrophys. J.*, *392*, 667.
Parker R. J. and Meyer M. R. (2012) *Mon. Not. R. Astron. Soc.*, *427*, 637.
Penston M. V. (1969) *Mon. Not. R. Astron. Soc.*, *144*, 425.
Peterson D. E. and Megeath S. T. (2008) *The Orion Molecular Cloud 2/3 and NGC 1977 Regions*, p. 590.
Pezzuto S. et al. (2012) *Astron. Astrophys.*, *547*, A54.
Pilbratt G. L. et al. (2010) *Astron. Astrophys.*, *518*, L1.
Pillitteri I. et al. (2013) *Astrophys. J.*, *768*, 99.
Pineda J. E. et al. (2011) *Astrophys. J.*, *743*, 201.
Pineda J. E. et al. (2012) *Astron. Astrophys.*, *544*, L7.
Pontoppidan K. M. et al. (2008) *Astrophys. J.*, *678*, 1005.
Poteet C. A. et al. (2011) *Astrophys. J. Lett.*, *733*, L32.
Poteet C. A. et al. (2013) *Astrophys. J.*, *766*, 117.
Price D. J. et al. (2012) *Mon. Not. R. Astron. Soc.*, *423*, L45.
Rebull L. M. et al. (2010) *Astrophys. J. Suppl.*, *186*, 259.
Robitaille T. P. et al. (2006) *Astrophys. J. Suppl.*, *167*, 256.
Saigo K. and Tomisaka K. (2006) *Astrophys. J.*, *645*, 381.
Saigo K. and Tomisaka K. (2011) *Astrophys. J.*, *728*, 78.
Saigo K. et al. (2008) *Astrophys. J.*, *674*, 997.
Sargent B. A. et al. (2009) *Astrophys. J. Suppl.*, *182*, 477.
Sauter J. et al. (2009) *Astron. Astrophys.*, *505*, 1167.
Schnee S. et al. (2012) *Astrophys. J.*, *745*, 18.
Schneider N. et al. (2012) *Astron. Astrophys.*, *540*, L11.
Schneider S. and Elmegreen B. G. (1979) *Astrophys. J. Suppl.*, *41*, 87.
Scholz A. (2012) *Mon. Not. R. Astron. Soc.*, *420*, 1495.
Scholz A. et al. (2013) *Mon. Not. R. Astron. Soc.*, *430*, 2910.
Schwarz K. R. et al. (2012) *Astron. J.*, *144*, 115.
Shakura N. I. and Sunyaev R. A. (1973) *Astron. Astrophys.*, *24*, 337.
Shu F. H. (1977) *Astrophys. J.*, *214*, 488.
Shu F. H. et al. (1987) *Annu. Rev. Astron. Astrophys.*, *25*, 23.
Stahler S. W. (1988) *Astrophys. J.*, *332*, 804.
Stahler S. W. et al. (1980) *Astrophys. J.*, *241*, 637.
Stamatellos D. et al. (2011) *Astrophys. J.*, *730*, 32.
Stutz A. et al. (2010) *Astron. Astrophys.*, *518*, L87.
Stutz A. M. et al. (2008) *Astrophys. J.*, *687*, 389.
Stutz A. M. et al. (2013) *Astrophys. J.*, *767*, 36.
Takahashi S. et al. (2013) *Astrophys. J.*, *763*, 57.
Takakuwa S. et al. (2012) *Astrophys. J.*, *754*, 52.
Tassis K. and Mouschovias T. C. (2005) *Astrophys. J.*, *618*, 783.
Terebey S. et al. (1984) *Astrophys. J.*, *286*, 529.
Tobin J. J. et al. (2010) *Astrophys. J.*, *712*, 1010.
Tobin J. J. et al. (2012) *Nature*, *492*, 83.
Tobin J. J. et al. (2013) *ArXiv e-prints*.
Tomida K. et al. (2010) *Astrophys. J. Lett.*, *725*, L239.
Tomisaka K. and Tomida K. (2011) *PASJ*, *63*, 1151.
Toomre A. (1964) *Astrophys. J.*, *139*, 1217.
van Broekhuizen F. A. et al. (2006) *Astron. Astrophys.*, *451*, 723.
van Kempen T. A. et al. (2009) *Astron. Astrophys.*, *498*, 167.
Visser R. and Dullemond C. P. (2010) *Astron. Astrophys.*, *519*, A28.
Visser R. et al. (2009) *Astron. Astrophys.*, *495*, 881.
Vorobyov E. I. (2009a) *Astrophys. J.*, *692*, 1609.
Vorobyov E. I. (2009b) *Astrophys. J.*, *704*, 715.
Vorobyov E. I. (2010) *New A*, *15*, 24.
Vorobyov E. I. (2011a) *Astrophys. J. Lett.*, *728*, L45.
Vorobyov E. I. (2011b) *Astrophys. J.*, *729*, 146.
Vorobyov E. I. (2013) *Astron. Astrophys.*, *552*, 129.
Vorobyov E. I. and Basu S. (2005) *Astrophys. J. Lett.*, *633*, 137.
Vorobyov E. I. and Basu S. (2006) *Astrophys. J.*, *650*, 956.
Vorobyov E. I. and Basu S. (2007) *Mon. Not. R. Astron. Soc.*, *381*, 1009.
Vorobyov E. I. and Basu S. (2008) *Astrophys. J. Lett.*, *676*, 139.
Vorobyov E. I. and Basu S. (2009) *Astrophys. J.*, *703*, 922.
Vorobyov E. I. and Basu S. (2010a) *Astrophys. J.*, *719*, 1896.
Vorobyov E. I. and Basu S. (2010b) *Astrophys. J. Lett.*, *714*, 133.
Werner M. W. et al. (2004) *Astrophys. J. Suppl.*, *154*, 1.
White R. J. et al. (2007) *Protostars and Planets V*, pp. 117–132.
Whitney B. A. et al. (2003a) *Astrophys. J.*, *591*, 1049.
Whitney B. A. et al. (2003b) *Astrophys. J.*, *598*, 1079.
Wilking B. A. et al. (1987) in: *Bulletin of the American Astronomical Society*, vol. 19 of *Bulletin of the American Astronomical Society*, p. 1092.
Winston E. et al. (2007) *Astrophys. J.*, *669*, 493.
Winston E. et al. (2010) *Astron. J.*, *140*, 266.
Wolf S. et al. (2008) *Astrophys. J. Lett.*, *674*, L101.
Wolk S. J. et al. (2013) *ArXiv e-prints*.
Wu J. et al. (2007) *Astron. J.*, *133*, 1560.
Yen H.-W. et al. (2013) *ArXiv e-prints*.
Yorke H. W. and Bodenheimer P. (1999) *Astrophys. J.*, *525*, 330.
Young C. H. and Evans II N. J. (2005) *Astrophys. J.*, *627*, 293.
Young C. H. et al. (2004) *Astrophys. J. Suppl.*, *154*, 396.
Zapata L. A. et al. (2013) *Astrophys. J. Lett.*, *764*, L14.
Zasowski G. et al. (2009) *Astrophys. J.*, *694*, 459.
Zhu Z. et al. (2009) *Astrophys. J.*, *694*, 1045.
Zhu Z. et al. (2010) *Astrophys. J.*, *713*, 1134.

This 2-column preprint was prepared with the AAS LaTeX macros v5.2.